Universiteit Utrecht

IMAU
Institute for Marine and Atmospheric research Utrecht

Faculteit Bètawetenschappen

The stratospheric final warming in relation to the spring amplification

Bachelor Thesis

Jonna van Mourik

Natuur- en Sterrenkunde

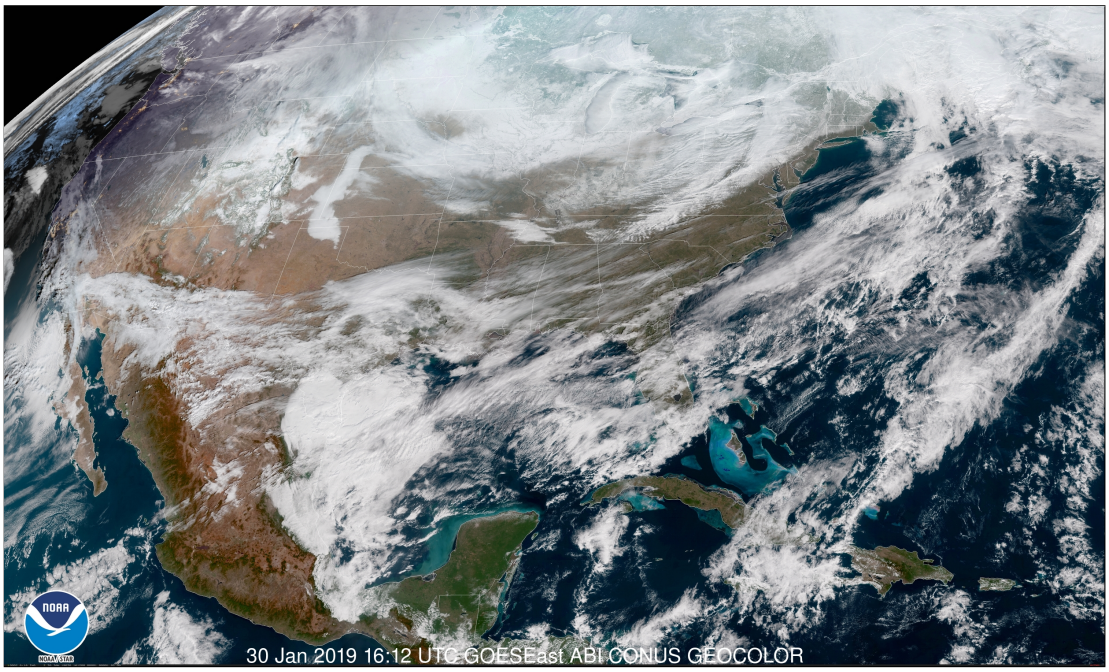

Supervisor:

Dr. A.J. van Delden
IMAU

June 2020

Abstract

In recent years, spring temperatures have been rising faster than yearly averaged temperatures. This spring amplification could be a result of the observed changed position of stationary waves near the surface of the earth. At the same time, it is observed that recently the seasons in the stratosphere, which is a layer of the atmosphere from approximately 10 to 50 km above the earth's surface, are changing from winter to summer later in the year. This change of seasons is characterized by the stratospheric polar vortex, which is cyclonic in winter and anticyclonic in summer. Our hypothesis is that the spring amplification has a connection to the delay of the stratospheric transition from winter to summer. Using re-analysis of the ERA-Interim data of ECMWF, we investigate the changes in the behaviour of the stratospheric polar vortex and look for relations between the spring amplification and the stratospheric polar vortex. Potential vorticity and planetary waves form the connection between the stratosphere and the troposphere and will be used to explain possible relations. It is found that the transition to summer in the stratosphere might be delayed, but the correlation is weak and thus it cannot be said with certainty. The time lag between the reversal in the higher and lower stratosphere shows more variation, the planetary wave activity plays a big role in the early onset dates for the final warming but not in the later onset dates, the northern annular mode index, indicating the pressure distribution, is not showing a trend in the months of March to May, and a significant relation between the date of the reversal of the stratospheric polar vortex and the mean index of the NAM over the period of March to May could not be found. Further research is needed to investigate the role of the strength of the polar vortex in relation to the NAM-index.

Contents

1 Introduction **1**

2 Theory **2**
2.1 The atmosphere . . . 2
2.2 The stratospheric polar vortex . . . 2
2.3 Planetary waves . . . 3
2.4 Northern annular mode . . . 5
2.5 Potential vorticity . . . 5

3 Methodology **8**
3.1 Data . . . 8
3.2 Interpolate pressure to potential temperature . . . 8
3.3 Determine the dates of the stratospheric final warming . . . 8
3.4 Planetary waves . . . 9
3.5 Northern annular mode . . . 9
3.6 Correlation between the reversal days, planetary waves and the NAM . . . 10

4 Results **11**
4.1 The reversal date of the potential vorticity anomaly . . . 11
4.2 The reversal date of the zonal mean zonal wind . . . 12
4.3 Extremely early and late reversal dates for u and PV* . . . 13
4.4 The propagation of the u and PV* reversal . . . 14
4.5 Planetary waves . . . 15
4.6 Northern annular mode . . . 18
4.7 Correlations between the reversal date, planetary waves and the NAM . . . 19

5 Discussion **23**
5.1 The reversal day of u and PV* . . . 23
5.2 Extremely early and late reversal dates for u and PV* . . . 23
5.3 The propagation of the u and PV* reversal . . . 23
5.4 Planetary waves . . . 23
5.5 Northern annular mode . . . 24

6 Conclusion **25**

A Values for the PV* reversal on different isentropic layers **26**

B Values for the u reversal on different isentropic levels **27**

References **II**

1 Introduction

In March this year, the national news platform NOS brought out the news that spring temperatures are increasing faster than any other season. This fact was also stated in the Fourth assessment Report of the IPCC by Parry et al. [1]. They found that since the 1970s, spring is beginning earlier in the mid- and high northern latitudes, thus leading to warmer averages in what we traditionally call the spring months. This spring amplification has an effect on many things, such as the timing of biological events [2], making it an interesting research topic. A good example is the arrival of migratory birds in the Europe. They plan their journey to arrive exactly when there is a peak in the amount of caterpillars, which depends on the moment the trees grow their leaves. With the spring amplification, the leaves start to grow earlier resulting in birds arriving when the caterpillars have long become butterflies.

Warmer temperatures can be caused by a lot op things. Some of them are better known than others, such as the amount of sunlight reaching the earth or the enhanced greenhouse effect. The wind direction also has a huge impact on our daily weather. Wind from the north causes colder temperatures than wind from the south, bringing warmer air towards us. These winds are regulated by differences in pressure, which can be influenced by stationary waves. The northern annular mode (NAM) index is a measure for the pressure difference between the pole and mid-latitudes. This index will be used as a measure for the spring amplification, as will be further explained in Section 2.4. In this research, we will focus our attention on the possible effects of the stratosphere and in particular the stratospheric polar vortex in the northern hemisphere on this spring amplification. Due to the polar vortex, we can define two seasons in the stratosphere, namely winter and summer. In winter, the polar vortex is cyclonic, while in summer the vortex is anticyclonic. The onset date is defined as the date when the vortex changes its direction. Recently, the stratospheric final warming turns out to have its onset date later than the years of the 1970s [3], causing the summer in the stratosphere to start later. This causes a strange contrast to the spring amplification in the northern hemisphere. Both phenomena can be related to the increased amount of carbon dioxide, warming the troposphere and cooling the stratosphere. Our hypothesis is that there exist a connection between the delay in the stratospheric transition to the summer season and the warmer temperatures in spring in the troposphere, both on the northern hemisphere. We evaluate the changes in the stratosphere and the troposphere over the years with respect to the onset date of the stratospheric final warming, the behaviour of planetary waves and the trends in the northern annular oscillation (NAM) index, using re-analysis. We will do this using the following research question:

What are the changes in the occurrence of the stratospheric final warming due to climate change and how do these changes explain the observed change in the position of stationary waves near the surface of the earth?

2 Theory

To get a clear view of the reasoning in this research, some background information is needed. We will start with a global picture of the atmosphere, explaining the differences between the stratosphere and the troposphere. Then we will take a closer look at the stratosphere and in particular the stratospheric polar vortex and the onset date of its break-up. Making the connection between the stratosphere and the troposphere, we will investigate the role of planetary waves, coming from the troposphere and their effect on the stratosphere. We will continue in the troposphere, explaining the working of the northern annular mode with respect to pressure areas and the winds resulting from them. We close this section off with the explanation of potential vorticity and how this quantity can help describe the above phenomena.

2.1 The atmosphere

In 1902, upon his discovery of the temperature inversion at the tropopause, the French meteorologist Léon Philippe Teisserenc de Bort (1855-1913) theorized the existence of a two layered atmosphere, where the tropopause formed the boundary between the troposphere below and the stratosphere above[4]. Nowadays, we know that the atmosphere exists of more layers. Nonetheless Teisserenc de Bort's discovery was of great importance. Seen from the earth's surface, the atmosphere consists of the troposphere, the tropopause, the stratosphere, the stratopause, the mesosphere, the mesopause, the thermosphere, ending with the ionosphere [5]. This research paper will focus its attention from the stratopause down to the troposphere and will explain the important characteristics of these layers.

The troposphere contains the largest amount of mass of all atmospheric layers. Since it is also the layer where almost all water vapour is situated, it's where we experience our daily weather phenomena. The temperature in the lower layer of the troposphere is relatively high due to the absorption of radiation by greenhouse gases and long wave radiation emitted by the earth's surface. Since the long wave radiation is emitted by the surface, the air right above is heated more effective than air higher in the troposphere, which is the reason for the temperature decrease with height. This decrease goes on until the tropopause, which is situated at a height of approximately 10 km, where the temperature gradient reverses. In the stratosphere, roughly between the 10 and 50 km, ozone absorbs solar radiation. Most of the ozone is situated at the top of the stratosphere, resulting in a stable situation with warm air above cooler air, as can be seen in Figure 1. Therefore, there is a lot less turbulence compared to the troposphere, leading to the long-time believe that the stratosphere does not contribute to our everyday weather system. Since some time, there is evidence that changes in the stratosphere actually do have an important and prolonged effect on the troposphere, although further research is still needed [6].

When looking at the effect of climate change due to an increase of greenhouse gases in the atmosphere [7], there are some interesting differences to be found between the troposphere and the stratosphere. As we can perceive, the increased concentration of carbon dioxide causes higher surface temperatures and thus higher tropospheric temperatures. At the same time, Rind et al. [8] shows that the same increase in carbon dioxide causes the stratosphere to become cooler during all seasons, although this cooling is slightly less in the region where the polar night occurs. This cooling effect is due to the increase in the amount of long wave radiation absorbers, such as carbon dioxide. They emit the long wave radiation in all directions, but due to the stratospheres placement high in the atmosphere, a lot of this radiation gets lost in space, resulting in lower stratospheric temperatures [9].

2.2 The stratospheric polar vortex

The first part of the atmosphere that we are going to focus on is the stratosphere. In both the northern- and the southern hemisphere a polar vortex is formed over the winter pole during their respective fall seasons. This is the time of year when the amount of solar radiation on the poles drops radically. This is due to the increased difference between the temperature at the poles and the equator, causing a low pressure area which results in a strong cyclonic vortex around the poles [10]. This vortex strengthens during the winter season and breaks down again in spring. In this research paper, we will only look at the northern hemisphere and focus on the breakdown of the vortex in spring.

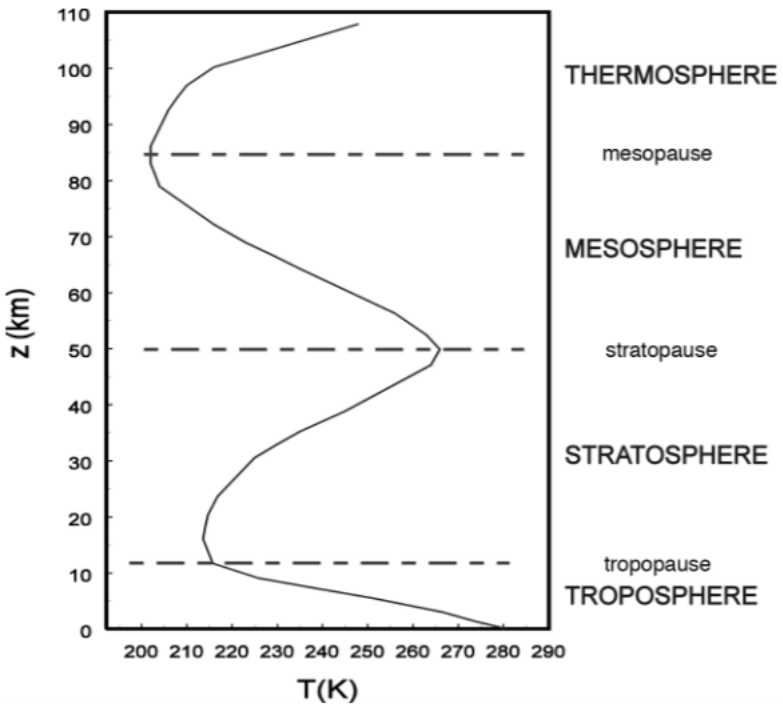

Figure 1: Vertical temperature profile for the "US standard atmosphere" at 40° N in December [5].

In midwinter, when the vortex has its greatest strength, sudden stratospheric warmings (SSWs) can happen. During such an event, the temperature at the winter pole increases rapidly, causing the polar vortex to lose speed [11]. Planetary waves play a huge role in the occurrence of sudden stratospheric warmings, as will be explained in Section 2.3. The breaking up of the polar vortex can result in two situations: the first is a shifted situation, where the polar vortex is displaced off the pole. The second is a split of the polar vortex into smaller vortices. This can be made clear using the potential vorticity, which is able to show the outer shape of the vortex and will be explained in Section 2.5. SSWs do not happen every year, but in around 65-91 percent of the years, depending on how the SSW is defined [12]. This does not exclude the possibility of having more than one SSW in one winter.

Something that does happen every year, without exception, is the stratospheric final warming (SFW). This is the last time that the stratospheric polar vortex becomes anticyclonic until the next fall.
The stratospheric final warming has a huge interannual variability. When we take the onset date of the SFW to be the day when the area-weighted mean zonal mean zonal wind $u < 0$ ms^{-1} at $p = 10$ hPa, averaged over 60°-90°, we end up with a mean date of day 99. This day corresponds to the 10$^{\text{th}}$ of April and it has a standard deviation of 19 days. This indicates that the onset date of the SFW varies between mid-March and early May. The date of the final warming has a strong coherence with the planetary wave activity and the presence of preceding sudden stratospheric warmings [13]. In the next section, we will take a closer look at the planetary waves.

2.3 Planetary waves

Planetary waves, or Rossby waves as they are often called, are waves propagating from the troposphere to the stratosphere due to the topography of land surfaces and temperature gradients. These planetary waves can only propagate from the troposphere to the stratosphere under certain conditions, which are stated in Equation 2.1. This equation has as a result that planetary waves can only propagate vertically for westerly winds between 0 and U_c.

$$0 < \bar{u} < \beta[(k^2 + l^2) + \frac{f_0^2}{4N^2H^2}]^{-1} \equiv U_c, \tag{2.1}$$

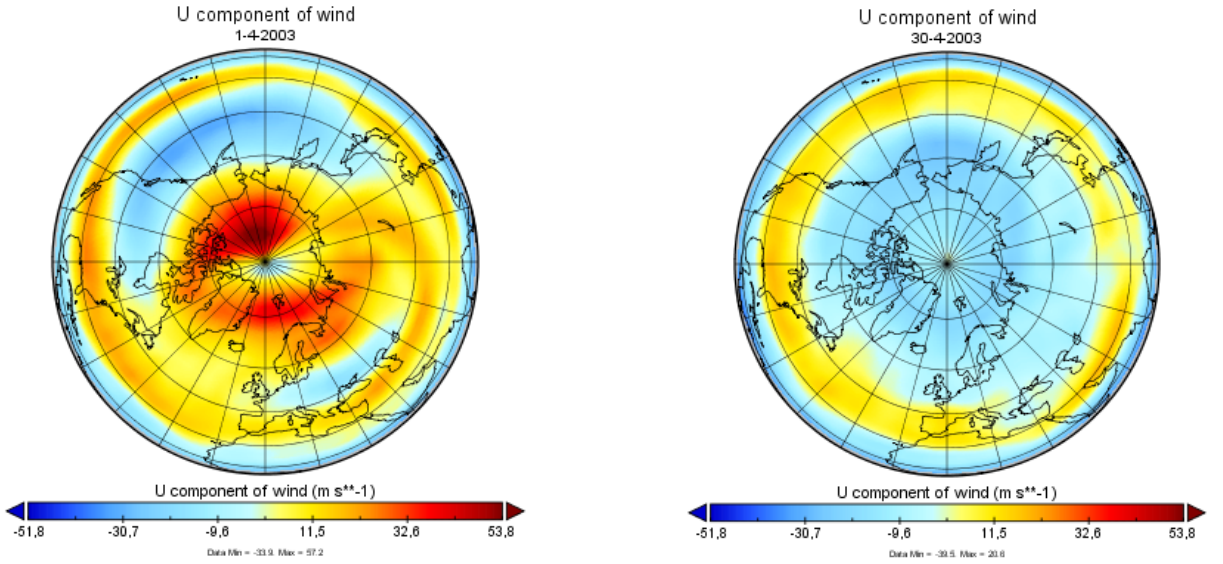

(a) (b)

Figure 2: The zonal wind velocity at $p = 10$ hPa for a) 1-4-2003 and b) 30-4-2003, based on the ERA-Interim reanalysis, `https://apps.ecmwf.int` and produced with Panoply.

where $\bar{u}$ is the zonal mean zonal wind, $\beta = \frac{df}{dy}$ the Rossby parameter where f stands for the Coriolis parameter, k and l the zonal and meridional wave number, f_0 a constant mid-latitude reference value for the Coriolis parameter, N the Brunt-Väisälä frequency, $H \equiv R < T > /g_0$ a layer mean scale height with T the temperature, g_0 the global average of gravity at mean sea level and R the gas constant for dry air and U_c the Rossby critical velocity. Since easterly winds have a negative $\bar{u}$, planetary waves cannot vertically propagate into the stratosphere after the stratospheric final warming [14].

The waves that do reach the stratosphere and are not reflected due to easterly winds or westerly winds exceeding the Rossby critical velocity, are mostly high amplitude and low wave-number waves, such as wave-number 1 and 2. They slow down the polar vortex by exerting a 'planetary wave drag', which might eventually even break the vortex down completely [15]. The activity of the planetary waves can be measured using the Eliassen-Palm (EP) flux [16]. For the horizontal and vertical component of the EP-flux, we have respectively

$$F_\phi = \rho a \cos\phi(-\bar{v'u'}) \tag{2.2}$$

and

$$F_z = \rho a f \cos\phi \bar{v'\theta'}(\frac{\partial\bar{\theta}}{\partial z})^{-1}, \tag{2.3}$$

where ρ is the atmospheric density, a the radius of the Earth, ϕ is the latitude, θ stands for the potential temperature, defined as

$$\theta = T(\frac{p_{ref}}{p})^\kappa, \tag{2.4}$$

with p_{ref} the reference pressure taken at 1000 hPa, p the pressure, κ the ratio R/c_p, where R is the specific gas constant of air and c_p the specific heat capacity of air. $\bar{v'}$ is the departure of the zonal mean meridional velocity, $\bar{u'}$ is the departure of the zonal mean zonal velocity, f is the earlier mentioned Coriolis parameter, $\bar{\theta'}$ the zonal mean anomaly of the potential temperature and $\bar{\theta}$ the zonal mean potential temperature. Equation 2.2 and Equation 2.3 show the activity of the planetary waves, where Equation 2.3 presents the meridional heat flux caused by the waves. An upward flux means that heat is transported from the equator to the Pole, while a negative flux means transport from the pole to the equator. The vertical component of the EP-flux often peaks before stratospheric final warmings and disappears relatively fast when the final warming reaches its onset date [17].

Together, the horizontal and vertical component form the Eliassen-Palm flux: $F = (F_\phi, F_z)$, of which we can take the divergence:

$$\Delta \cdot \vec{F} = (a\cos\phi)^{-1}\frac{\partial}{\partial\phi}(F_\phi \cos\phi) + \frac{\partial F_z}{\partial z}. \tag{2.5}$$

The divergence of this flux has an important effect on the mean flow, since the zonal mean zonal wind velocity accelerates when the Eliassen-Palm flux diverges and decelerates when it converges [18]. Due to this relation, a minimum can often be found days before a stratospheric final warming, decelerating the zonal mean zonal wind and leading to the reversal of the westerly winds [17].

2.4 Northern annular mode

The northern annular mode (NAM) is defined as

$$\text{NAM} = \hat{P}_{35^\circ N} - \hat{P}_{65^\circ N}, \tag{2.6}$$

where $\hat{P}_{35^\circ N}$ is the zonal mean monthly mean sea level pressure for 35°N and $\hat{P}_{65^\circ N}$ for 65° N. They represent respectively the strength of the pressure field at the subtropical high and of the sub-polar low and the result is the normalized NAM index. When we are dealing with a positive NAM index, the Pole has a lower pressure than usual, while at the same time pressure at the subtropics is higher. For the negative index, this is the other way around. There is also a connection between the NAM-index and the EP-flux. During the negative phase, EP-fluxes are much more drawn towards the Pole than during a positive phase, when the EP-flux is more directed upward and equatorward. As a result, the stratospheric polar vortex becomes weaker when a positive phase of the NAM persists [19]. In general, the NAM is therefore positive before the SFW and negative after the SFW [20]. In the winter season, a positive phase generally leads to warmer and wetter weather in the northwest of Europe due to an enhanced westerly wind, while the negative phase leads to colder and drier weather as a result of a more easterly wind [21]. In the summer season however, a positive NAM index will lead to warmer and drier weather above Europe and a negative NAM index results in colder and wetter conditions.

Other ways of defining the pressure difference between the Pole and the subtropics that are often used in research, are the Arctic Oscillation (AO) and the North Atlantic Oscillation (NAO). The AO is basically the same as the NAM, while the NAO is really something different, although it has a high correlation to the NAM. As is in the name, the NAO is limited to the North Atlantic region between Greenland and Europe. The places that are taken for the pressure differences are a site in Iceland and one in the Azores [22]. Besides their different names, the research papers done on the AO and the NAO can be used to argue the trends in the NAM as a result of their strong coherence.

2.5 Potential vorticity

In this research, we will use the potential vorticity for the determination of the SFW. Potential vorticity (or isentropic potential vorticity, which indicates the same in this paper) is defined as

$$Z_\theta = \frac{\zeta_\theta + f}{\sigma} = -g(\zeta_\theta + f)\frac{\partial\theta}{\partial p}, \tag{2.7}$$

where ζ_θ is the isentropic relative vorticity defined as

$$\zeta_\theta = (\frac{\partial v}{\partial x})_\theta - (\frac{\partial u}{\partial y})_\theta, \tag{2.8}$$

with v the meridional wind velocity and u the zonal wind velocity in an isentropic coordinate system. f is the earlier mentioned Coriolis parameter, also named the planetary vorticity and σ [kg m^{-2} K^{-1}] is the isentropic density defined as

$$\sigma = -\frac{1}{g}\frac{\partial p}{\partial\theta}. \tag{2.9}$$

In short, potential vorticity is a measure of vorticity, weighted by the mass of density, where we take vorticity as the curl of the velocity vector. Potential vorticity is expressed in potential vorticity units, PVU's, which have the expressed in PVU = 10^{-6} $\mathrm{Km^2kg^{-1}s^{-1}}$. Potential vorticity is a very useful measure in the atmosphere when it comes to the dynamics of it, since it can show the division of the atmosphere in different layers and also point out bigger vortices. In the case of the stratospheric polar vortex, an area of high potential vorticity can be found over the poles, due to the diabatic[1] cooling of the atmosphere. When the polar vortex breaks up, this high potential vorticity region changes into a low potential vorticity region due to diabatic heating in combination with the interference of planetary waves. These waves mix the higher than normal potential vorticity inside of the vortex with the lower than normal potential vorticity on the outside of it. This can be seen in Figure 3, which is taken for the same year and date as Figure 2. At the beginning of the month, before the final warming, there is a relatively high potential vorticity, while at the end of the month, after the final warming, this higher potential vorticity has completely disappeared. The effect of diabatic

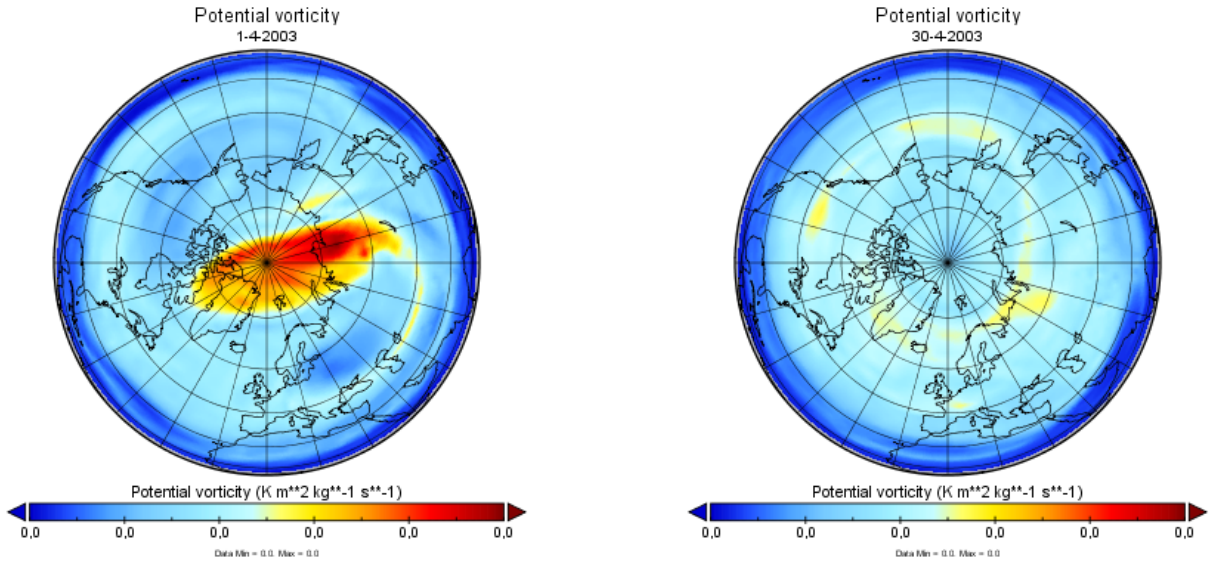

(a) (b)

Figure 3: The potential vorticity at $p = 10$ hPa for a) 1-4-2003 and b) 30-4-2003, Based on the ERA-Interim reanalysis, `https://apps.ecmwf.int` and produced with Panoply.

heating and cooling on the potential vorticity can be derived from the potential vorticity equation, where friction- and tilting-terms are neglected:

$$\frac{\partial Z_\theta}{\partial t} + u(\frac{\partial Z_\theta}{\partial x})_\theta + v(\frac{\partial Z_\theta}{\partial y})_\theta = -\frac{d\theta}{dt}\frac{\partial Z_\theta}{\partial \theta} + Z_\theta \frac{\partial}{\partial \theta}\frac{d\theta}{dt}. \tag{2.10}$$

When the winter season starts at the North Pole, $\frac{d\theta}{dt}$ becomes smaller than zero, while the term $\frac{\partial Z_\theta}{\partial \theta}$ is positive. This first term on the right hand side accounts for the diabatic advection of the potential vorticity. The second term accounts for the stretching effect on the potential vorticity and doesn't always have to be positive. In general, the winter season thus leads to a higher potential vorticity and vice versa in summer. Under adiabatic circumstances however, air-parcels conserve their potential vorticity and therefore have to stay on their specific isentropes. The best way to describe the deviation of the potential vorticity is with the potential vorticity anomaly, which is defined as the potential vorticity minus a reference potential vorticity divided by this reference potential vorticity

$$PV* = \frac{Z - Z_{ref}}{Z_{ref}}. \tag{2.11}$$

[1]Diabatic: involving the transfer of heat

We will refer to the potential vorticity anomaly using PV*. Since there is a positive PV* when the polar vortex is cyclonic and a negative PV* when the polar vortex is anticyclonic, there must be a relation between the PV* and the zonal wind velocity. This relation is given in the form of the invertibility principle for potential vorticity, which is a non-linear differential equation. It represents the thermal wind balance, but in terms of potential vorticity. The original thermal wind balance is shown in Equation 2.12.

$$\frac{\partial \Pi}{\partial r} = (f + \frac{2u}{r})\frac{\partial u}{\partial \theta}, \tag{2.12}$$

here, $\Pi = \frac{\partial \Psi}{\partial \theta}$, where Ψ is the Montgomery streamfunction $\Psi = gz + c_pT$. Expressed in terms of potential vorticity, we end up with

$$\frac{\partial}{\partial r}(\frac{1}{r}\frac{\partial ur}{\partial r}) + \frac{Z}{g}\frac{\partial}{\partial \theta}(\rho\theta(f + \frac{2u}{r})\frac{\partial u}{\partial \theta}) = \sigma\frac{\partial Z}{\partial r}. \tag{2.13}$$

Since Equation 2.13 is non-linear, it can't be solved analytically, only numerically. A solution was found by Kleinschmidt in 1957 [23], which showed that, among others, an air mass with a positive PV* gives rise to a cyclone and a negative PV* to an anticyclone, just as is visible during the forming and breaking down of the polar vortex [24]. A complete numerical derivation of the invertibility principle can be found in the research paper of Van Delden and Hinssen [25].

3 Methodology

3.1 Data

For this re-analysis, we use the data provided by the ECMWF, which stands for the European Centre for Medium Range Weather Forecasts, where we made use of the ERA-I, the Interim Re-analysis dataset [26]. This dataset covers the years of 1979-2019, which will all be used. For every year, we take the months of March, April and May, covering the boreal spring months. All the data is taken from $p = 1000$ hPa to $p = 1$ hPa divided over 37 levels for every 6 hours. The area that is covered runs from $\phi = 90°$N to $\phi = 10°$ N with a resolution of 2.5°x2.5°. The parameters included are the geopotential, potential vorticity, temperature, zonal and meridional components of the wind and relative vorticity.

3.2 Interpolate pressure to potential temperature

Before we get to the re-analysis of the chosen parameters, we first interpolate the dataset from pressure (p) to the potential temperature (θ) as the vertical coordinate. The use of an isentropic coordinate system instead of an isobaric coordinate system has a few reasons. One of them being the distribution of the isentropes over height in the stratosphere. When working in an isobaric coordinate system, the focus is on the troposphere, since the stratosphere expands from $p \sim 100$ hPa to $p \sim 1$ hPa, while the troposphere expands from $p \sim 1000$ hPa to $p \sim 100$ hPa. From the definition of potential temperature, $\theta = T(\frac{P_0}{P})^{R/C_p}$, where T is the temperature in Kelvin, P_0 is the reference pressure, R is the specific gas constant of air and C_p the specific heat capacity of air, we can see that, due to the increasing temperature in the stratosphere and the decreasing pressure, the potential temperature increases more rapidly compared to the troposphere, putting the focus on the stratosphere. Other reasons for using the isentropic coordinate system instead of an isobaric coordinate system, are the facts that potential vorticity is conserved on isentropes under adiabatic circumstances and potential vorticity substance (PVS) cannot cross isentropes and thus always stays on isentropes due to the impermeability theorem [27].

For the interpolation of pressure to potential temperature, we choose to let the potential temperature run from $\theta = 295$ K to $\theta = 1255$ K in steps of 10 K, such that the centers of the layers are at respectively $\theta = 300$ K and $\theta = 1250$ K. From the interpolated pressure, the zonal mean can be calculated of the zonal wind component, the pressure at isentropes, the relative vorticity, the potential vorticity and the isentropic density on the different isentropic levels and layers and are saved to use in the further analysis.

3.3 Determine the dates of the stratospheric final warming

Just as is the case for sudden stratospheric warmings (SSW), the way the SFW is defined differs with almost every research article you find [12]. One of these methods is to define the SFW when the zonal mean zonal wind at 60° N becomes smaller than zero and thus changes from a westerly wind to an easterly wind at the height of $p = 10$ hPa, as is done by Lee and Butler [21]. A small variation is done by Wei, Chen, and Huang [3], where it is defined as $u < 0$ ms^{-1} at 10 hPa and 65°N. Black and McDaniel [20] choose a different place to define the SFW, namely at 50hPa and 70°N, while Nash et al. [28] choose a totally different way, namely using Ertel's potential vorticity. There, the SFW is defined as follows: Between 80°N and 50°N, $\theta = 450$ K and $u < 15.2$ ms^{-1}.

In this research, we will make use of both the potential vorticity anomaly and the zonal mean zonal wind velocity to get an extensive picture of the final warming events. Instead of working on just one isentropic level (layer), we chose to work on a few more to gain information about the development of the vortex. Here, it is important to note that the zonal mean zonal wind is calculated on isentropic levels and the potential vorticity in isentropic layers. We will choose the layers and levels such that they can be compared to each other. The first level we choose to work with, is the $\theta = 855$ K. This level is a good representation of the $p = 10$ hPa level and according to Butler and Gerber [29], this level is situated in the optimal range to determine the onset date of the SFW. The corresponding isentropic layer is taken to be $\theta = 840 - 850$ K, such that the mean of the layer is the used level. The other levels and layers are chosen around this central isentropic level. We've chosen to work with five levels (layers) in total, which turned out to be $\theta = 1195$ K ($\theta = 1190 - 1200$

K), representing the upper stratosphere, $\theta = 645$ K ($\theta = 640 - 650$ K), representing the lower stratosphere, and a level (layer) in between, namely $\theta = 1045$ K ($\theta = 1040 - 1050$ K). For each of these levels (layers) we define the onset date of the stratospheric final warming to be the the date when the area-weighted mean of the zonal mean zonal wind velocity (potential vorticity anomaly) between $\phi = 60°$N and $\phi = 90°$N becomes negative. In addition to this definition, we put the condition that, whenever the velocity (potential vorticity anomaly) becomes positive again and the duration is more than 10 days, the onset date is seen as a sudden stratospheric warming and not the final warming. Again, there is no consensus about the length of the period separating SSW's and SFW's. Hu et al. [13] uses five days for this separation, while Butler and Gerber [29] uses 20 days, so we chose something in between.

The scripts for the potential vorticity anomaly (PV*) and the zonal mean zonal wind velocity (u) both have the same structure. For all 3 months in the 41 years, the data is used that came out of the interpolation from pressure to potential temperature. For the dates, we keep the leap years in mind and start with the first day of January as day 0. For all the PV* and u values, it is checked whether they are positive or negative. Only the negative values are of interest and are kept for further inspection. For all these negative values, the day of occurrence is checked. If there are more than 10 days in between two negative values, the first negative value after this period is taken to be the SFW. If, however, a new period of more than 10 days is to be found after this date, again the first negative value is taken to be the onset date of the SFW. This is done for all five isentropes. This method is repeated for all three months evaluated per year, resulting in one onset date per year per isentropic level or layer for respectively u and PV*.

3.4 Planetary waves

Planetary waves form a connection between the stratosphere and the troposphere. To find the effect of planetary waves on the stratospheric final warmings and the delay in its onset date, we look at the vertical component of the Eliassen-Palm flux, representing the meridional flux of heat. High activity leads to a planetary wave drag, which will slow down the zonal mean zonal wind and thus can lead to a reversal in the wind velocity: the SFW. We will also look at the divergence of the EP-flux, which is important since negative divergences decelerate the mean flow. To evaluate the activity and divergence of the EP-flux, we use the same dataset as used before, except now we use the data in the isobaric system. We've chosen to work in the isobaric system, since we didn't include the meridional velocity in the interpolation from pressure to potential temperature. To make comparisons as good as possible, we decided to use the pressure levels of $p = 3$ hPa to represent $\theta = 1195$ K, $p = 5$ hPa to represent $\theta = 1045$ K and $p = 10$ hPa for $\theta = 845$ K, which come down to approximately the same height in the stratosphere. Below $p = 10$ hPa, the choice in pressure levels became smaller. We decided on $p = 20$ hPa for $\theta = 645$ K.

On these four pressure levels, we will work with the theory written by Edmon Jr, Hoskins, and McIntyre [30]. This results in values for the vertical component and the divergence of the Eliassen-Palm flux, for which we will look at the years of 1979-2019 by averaging the values all specific dates over the years. In addition, we will also analyse the variance in the vertical component and the divergence of the EP-flux by subtracting the minimum amplitude and divergence from the maximum amplitude and divergence for every year.

3.5 Northern annular mode

For the NAM-index, we used the measurements from Li and Wang [31] where the daily northern hemisphere annular mode index is defined for the years of 1948-2018, of which we will use the years 1979-2018. We will thus be missing the NAM-index for our last year in this re-analysis, 2019. To see if there are any trends in the values of the NAM-index, we average the NAM for every year over the full year, over the months March to May and over March, April and May separately. In Section 2.4, it is stated that the NAM-index is generally positive the days before the final warming and negative afterwards. If the final warming happens to have its onset date later in the year, we would expect the NAM-index of April to become on average more positive, due to the assumed delay of the negative NAM-index.

3.6 Correlation between the reversal days, planetary waves and the NAM

To find any correlations between the zonal mean zonal wind reversal day, the potential vorticity anomaly reversal day, the propagation of the reversal of the zonal mean zonal wind, the planetary waves and the northern annular mode, we plot the data of the different subjects against each other and determine their trend line using the least squares approximation for a linear fit. For the correlation coefficient, the r-value is used from the Pearson's correlation coefficient [32], where a value of +1 or -1 indicates perfect correlation and a value of 0 no correlation at all. The standard error of the correlation coefficient will be calculated according to Rowntree [33]. We will do this for the reversal date of u against the reversal date of the PV*, both methods for measuring the planetary wave activity against both reversal dates, both methods for measuring the planetary wave activity against the NAM-index and both reversal dates against the NAM-index.

4 Results

4.1 The reversal date of the potential vorticity anomaly

To determine the onset date of the stratospheric final warming, we first look at the potential vorticity anomaly. The date that the potential vorticity anomaly reverses from positive to negative, is plotted for every year

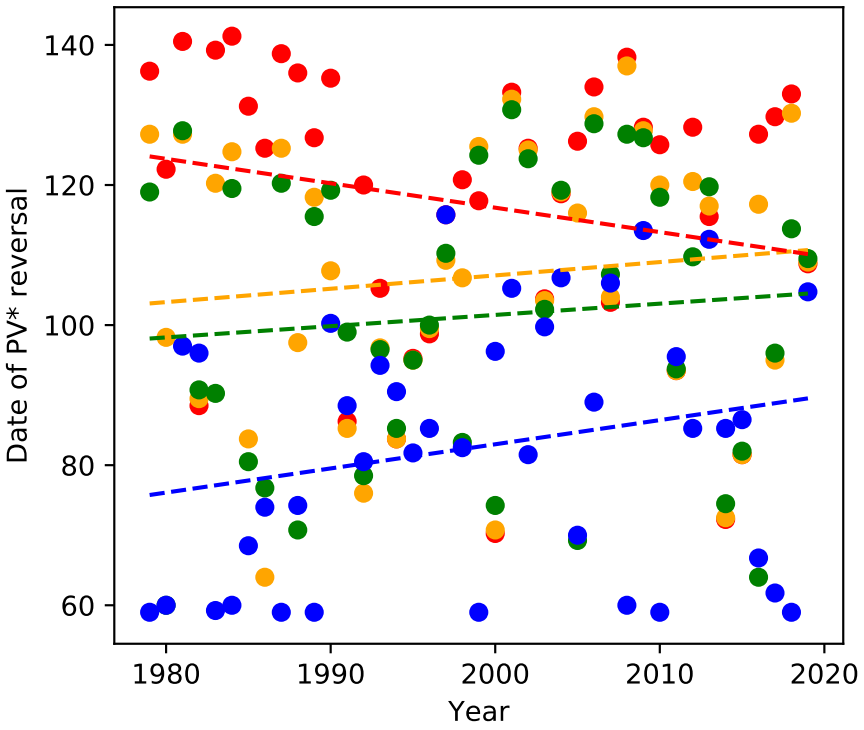

Figure 4: The reversal date of the area-weighted mean potential vorticity anomaly over 60°-90°N against the years, from 1979 to 2010. The isentropic layer for which the PV* reverses, is given in blue for $\theta = 640 - 650$ K, green for $\theta = 840 - 850$ K, orange for $\theta = 1040 - 1050$ K and red for $\theta = 1190 - 1200$ K. The corresponding trend lines have the same colour.

and for four isentropic layers in Figure 4. The first thing to notice is the variability of the dates of reversal of the PV*. All the dots are widely spread out over the months of March, April and May. When we look at the trend lines, we can see that generally, the further we go up in the stratosphere, the later the reversal date of the PV* takes place. For the layer of $\theta = 640 - 650$ K, the mean reversal date is date 83 (25 March) with a standard deviation of 18 days, for $\theta = 840 - 850$ K day 101 (12 April) with a standard deviation of 21 days, for $\theta = 1040 - 1050$ K day 107 (18 April) with a standard deviation of 19 days and for $\theta = 1190 - 1200$ K day 117 (28 April) with a standard deviation of 21 days. The variability around the mean date is for every isentropic layer approximately the same.

Again looking at the trend lines, we can see that the trend line for the highest layer is the only one with a negative gradient, while the middle three have a positive gradient. The gradient for $\theta = 1190 - 1200$ K is -0.35 days year^{-1} and the correlation coefficient is $r = -0.21 \pm 0.15$, for $\theta = 1040 - 1050$ K it is 0.19 days year^{-1} and $r = 0.12 \pm 0.15$, for $\theta = 840 - 850$ K it is 0.16 days year^{-1} and $r = 0.09 \pm 0.15$ and for $\theta = 640 - 650$ K it is 0.34 days year^{-1} and $r = 0.23 \pm 0.15$. Based on these gradients and the potential vorticity equation, we would expect the zonal mean zonal wind to start reversing at the lower isentropic levels and end at the higher isentropic levels, while the date of this reversal will, on average, be postponed over the years, except

for the highest layer, which might reverse earlier. The correlation coefficients however are very weak to weak for all trend lines, something that was already suggested by the big variability of the reversal dates.

4.2 The reversal date of the zonal mean zonal wind

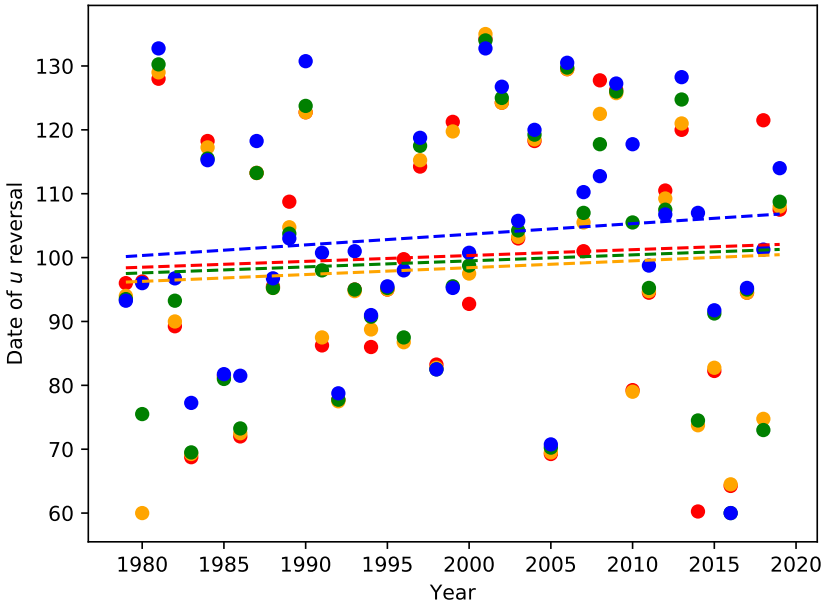

Figure 5: The reversal date of the area-weighted mean zonal mean zonal wind velocity over 60°-90°N against the years, from 1979 to 2010. The isentropic layer for which u reverses, is given in blue for $\theta = 645$ K, green for $\theta = 845$ K, orange for $\theta = 1045$ K and red for $\theta = 1195$ K. The corresponding trend lines have the same colour.

The next thing we will look at, is the area-weighted mean zonal mean zonal wind velocity reversal date over $60° - 90°$N, which can be seen in Figure 5. Just as with the reversal dates of the PV*, the variability of the reversal date of the zonal mean zonal wind is quite high, spreading over the full range of March, April and May. Now we go through the same checkpoints as for the PV*. For the PV*, we had a clear relationship between the height in the stratosphere and the reversal date. For the reversal date of u, this isn't as straightforward. The trend lines of the isentropic levels of $\theta = 1045$ K, $\theta = 845$ K and $\theta = 1195$ K almost lay on top of each other, the trend line of $\theta = 645$ K is placed just a bit above these three. Thus, on average, the zonal mean zonal wind reverses first at $\theta = 1045$ K with a mean date of 98 (9 April) and a standard deviation of 20 days, then at $\theta = 845$ K, with a mean date of 99 (11 April) and a standard deviation of 19 days, thereafter at $\theta = 1195$ K, with a mean date of 100 (12 April) and a standard deviation of 20 days and last at $\theta = 645$ K, with a mean date of 103 (15 April) and a standard deviation of 18 days. Just as for the potential vorticity anomaly, the variability is roughly the same for all isentropic levels.

When looking at the trend lines for the different isentropic levels, all lines are ascending. The gradients and correlation coefficients of the trend lines are for $\theta = 645$ K 0.17 days year^{-1} and $r = 0.11 \pm 0.15$, for $\theta = 845$ K 0.09 days year^{-1} and $r = 0.06 \pm 0.16$, for $\theta = 1045$ K 0.11 days year^{-1} and $r = 0.06 \pm 0.16$ and for $\theta = 1195$ K also 0.09 days year^{-1} and $r = 0.05 \pm 0.16$. As a result, the wind reversal at the middle and higher stratosphere are on average four to seven days later in 2019 than in 1979. The correlation coefficients are very weak, even compared to the correlation coefficients for the PV*.
Something that is not immediately visible when plotting all four isentropic layers in one plot, are the patterns in the reversal date for the specific isentropic layers. When plotting them as a histogram, this pattern becomes

more visible. The result can be seen in Figure 6 for the zonal mean zonal wind velocity for all five isentropic

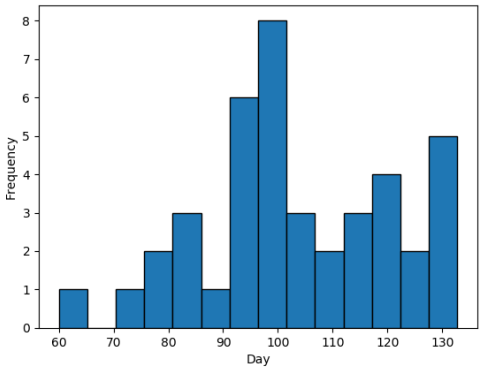

(a) $\theta = 645$ K

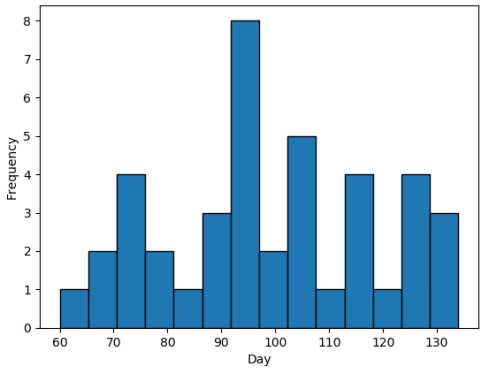

(b) $\theta = 845$ K

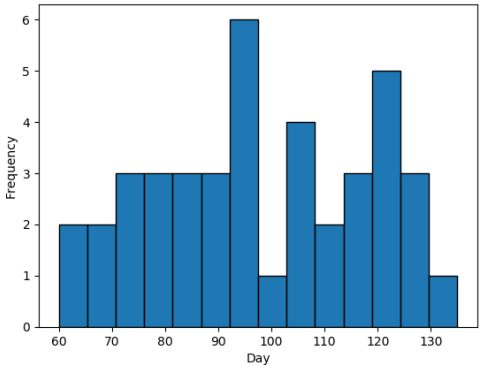

(c) $\theta = 1045$ K

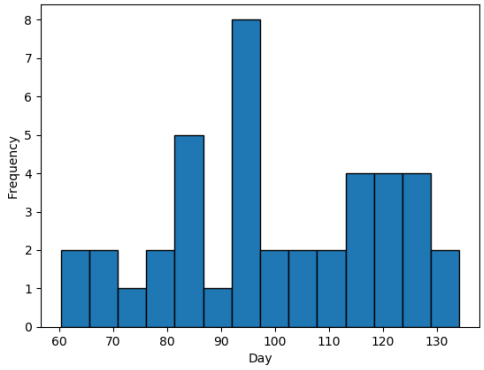

(d) $\theta = 1195$ K

Figure 6: The occurrence of the area-weighted mean zonal mean zonal wind over $60° - 90°$N reversal date between 1979 and 2019 for a) $\theta = 645$ K, b) $\theta = 845$ K, c) $\theta = 1045$ K and d) $\theta = 1195$ K.

levels. For Figure 6b, we can distinguish two peaks, namely around day 90-100 and 120-130, for Figure 6c has peaks around day 95 and 125-135 and a few lone peaks at 75, 105 and 115, Figure 6d has the peaks around day 95-105 and between 115 and 130, and finally Figure 6 has its peaks around day 95 and between 115 and 130. Although on some levels there are more than two peaks to be pointed out, we can still see some similarities. For all levels, there turn out to be more than average reversal days around day 95 (6 April) and day 125 (6 May). When we plotted the same series for the reversal date of the potential vorticity anomaly, nothing other than what we already saw in Figure 4 came out of it, namely that in the lower isentropic layers the reversal date was earlier than in the higher isentropic layers.

4.3 Extremely early and late reversal dates for u and PV*

After the global trend of PV* and u, we now take a closer look at the individual years to see if there are notable deviations from this trend. Since there are way to much dots in Figure 4 and 5 to make accurate comparisons, we printed the values for PV* and u, which can be found in Appendix A and B. We start with the values for the reversal date of u in Table 2. First, we will determine which years fall under the category of extremely early and extremely late years. For this, we will look at the $\theta = 845$ K level, since this is one laying closest to the more generally used definition of the SFW. The years with reversal dates above the mean date plus the standard deviation will be seen as the late years, while the mean minus the standard deviation will be used for the early years. This comes down to respectively day 99+19=118 and day 99-19=80. The years that fall under the first, late, category are 1981 (day 130.25), 1990 (day 123.75), 2001 (day 134.00), 2002

(day 125.00), 2005 (day 131.25), 2006 (day 129.75), 2009 (day 126.00) and 2013 (day 124.75). The years that fall under the early category are 1980 (day 75.5), 1983 (day 69.50), 1986 (day 73.25), 1992 (day 77.75), 2014 (day 74.50), 2016 (day 60.00) and 2018 (day 73.00). For the late years, this means that there are two late SFWs before 2000 and 6 after 2000. In the early years, it's more evenly divided with 4 before the 2000s and 3 after.

For the PV* we will, just as we did for the reversal date of u, look at the $\theta = 840 - 850$ K layer. Since the mean date for this layer was 101 with a standard deviation of 21 days, we take the early years to be before day 80 and the late years to be after day 122. The years that fall under the later years, are 1981 (day 127.75), 1999 (day 124.25), 2001 (day 130.75), 2002 (day 123.75), 2006 (day 128.75), 2008 (day 127.25) and 2009 (126.75). For the early reversals, the years are as follows: 1980 (before day 60.00), 1986 (day 76.75), 1988 (day 70.75), 1992 (day 78.50), 2000 (day 74.25), 2005 (day 69.25), 2014 (day 74.50) and 2016 (day 64.00). When we look at the late years, there are 7 years in total, of which 2 have taken place before 2000 and 5 after, which is approximately the same division as for the zonal mean zonal wind reversal. For the early years, there are 8 cases of which 4 before 2000 and 4 after and thus more evenly divided as was the case for u as well.

4.4 The propagation of the u and PV* reversal

Second, we look at the development of the onset date of the final warming. Some years seem to start their reversal in the lower stratosphere, while others start higher in the stratosphere or everywhere roughly at the same time. For this, we will look at the difference between the reversal date at $\theta = 1195$ K and $\theta = 645$ K. When the difference between the layers is positive, the final warming progresses from the lower to the higher stratosphere and when it is negative the other way around. It turns out that the mean difference between the two layers is -3.25 days, so most of the years must propagate from high to low. In total 9 years began their reversal at the lower stratosphere, 19 at the higher stratosphere and 13 reversed everywhere withing the range of 2 days and can thus be seen as reversing at the same time. These years are, for the reversal from low to high, 1979, 1984, 1989, 1993, 1999, 2008, 2012, 2016 and 2018. From high to low were 1981, 1982, 1983, 1986, 1987, 1990, 1991, 1994, 1997, 2000, 2002, 2003, 2007, 2010, 2011, 2013, 2014, 2015 and 2019. The years that reversed simultaneously are 1980, 1985, 1988, 1992, 1995, 1996, 1998, 2001, 2004, 2005, 2006, 2009 and finally 2017. From these years, there are 5 extreme years when taking the standard deviation of 11.88 in consideration. These years are 1999, when the higher stratosphere reversed 26 days later than the lower stratosphere, 2008, which had a 15 days difference, 2010 had a -38.5 days difference, 2014 had a -46.75 days difference and 2018 a 20.25 days difference. No extreme years happened in the first 20 years of our reanalysis.

Looking at the development of the PV* reversals at the different isentropic layers, we find that almost all years start their reversal in the lower stratosphere and work their way up, just as we saw in Figure 4. The mean difference between the $\theta = 1190 - 1200$ K and $\theta = 640 - 650$ K layers, is the large number of 34.15 days. The standard deviation is even more impressive with 32.57 days. The few years that do propagate from the higher stratosphere to the lower stratosphere, are 1982, 1991, 1994, 2000, 2007, 2011, 2014 and 2015. The year of 1997 reversed everywhere at the exact same time. 2000 and 2014 are the only years in this list that we've seen before in the early years of the $\theta = 840 - 850$ K PV* reversal. Now looking at the extremes, we use the sum of the mean and the standard deviation for the years with a large positive difference between the chosen layers and the difference between the mean and the standard deviation for the years with a large negative difference between them. There are a lot more extreme years than for the u reversal, which was to be expected due to the high standard deviation. 1979 has a 77.25 days difference, 1982 has -7.50 days, 1983 has 80.00 days, 1984 81.25 days, 1987 has 79.75 days, 1989 has 67.75 days, 1991 has -2.25 days difference, 1994 -6.75 days, 1997 the already mentioned 0 days, 2000 has a -26.00 days difference, 2007 -2.75 days, 2008 78.25 days, 2010 has 66.75 days, 2011 has -2 days, 2014 has -26.25 days, 2015 -5.00 days, 2017 68.00 days and finally 2018 74.00 days. It sounds quite strange to call a zero day difference and the comparable ones extreme years, but this is caused by the high variability of sometimes more than two months.

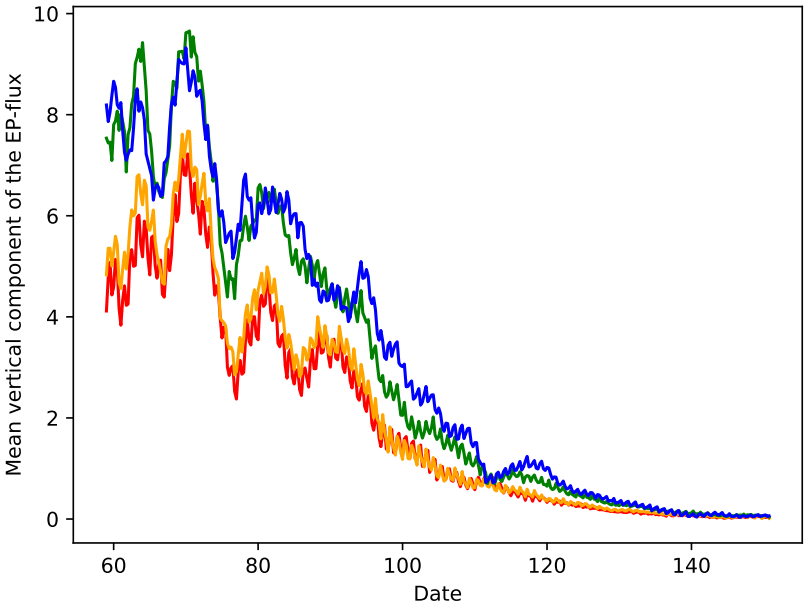

Figure 7: The mean vertical component of the EP-flux [(10^5 m^3s^{-2})] over 1979-2019 from March to May over the area of 90°N to 60°N. Red indicates $p = 3$ hPa, orange $p = 5$ hPa, green $p = 10$ hPa and blue $p = 20$ hPa.

4.5 Planetary waves

To find the effect of the planetary waves on the zonal mean zonal wind and potential vorticity anomaly reversal, we look both at the amplitude of the vertical component of the EP-flux and the divergence of the EP-flux. Note that we've used pressure coordinates here, as explained in Section 3.4. First, we will look at the vertical EP-flux. As can be seen in Figure 7, where the mean vertical component of the EP-flux is plotted for the years of 1979-2019, the EP-flux is at first relatively high and then makes its way, albeit via some small detours, to zero. In Section 2.3 it is explained that the higher levels of the stratosphere have smaller amplitudes than the middle and lower stratosphere, but the differences between them become smaller as they are approaching zero. For all levels, there are some peaks around day 63, a fall around day 67, a rise near day 70, followed by a bigger fall around day 77, a smaller rise at day 80, one last fall near 85, a last small rise around day 90 and than finally a continued negative gradient until zero is reached. Since this is the mean state over 41 years, not every year has this same pattern of height of amplitude. To see the differences over the years, we plotted the variability of the vertical component of the EP-flux against time, as can be seen in Figure 8. The variability for one year is taken to be the difference between the highest and the lowest EP-flux value in that specific year. The mean variance and standard deviation for the levels are for $p = 3$ hPa 20 ± 12, for $p = 5$ hPa 23 ± 14, for $p = 10$ hPa 29 ± 18 and for $p = 20$ hPa 27 ± 16, all in the units of [10^5 m^3 s^{-2}]. From the plot we can see that the amount of years with a bigger variance increases, leading to positive gradients in the trend lines of, from the highest level to the lowest, 0.20, 0.20, 0.25, 0.15 and 0.01 10^5 m^3 s^{-2} $year^{-1}$. The corresponding correlation coefficients are $r = 0.20 \pm 0.15$, $r = 0.16 \pm 0.15$, $r = 0.17 \pm 0.15$, $r = 0.12 \pm 0.15$ and $r = 0.01 \pm 0.16$. These all indicate a low correlation as was expected due to high variability between the years. We now again look at the extreme years, both the ones with a lot of variance and low variance, at the level of $p = 10$ hPa, since this corresponds to the $\theta = 845$ K used earlier. The years with a variance higher than 47 will be seen as high variance years and years with a variance lower than 11 will be seen as the low variance years. The high years are 1986, 2000, 2003, 2007, 2014, 2015 and 2016. The low years are 1987, 1989, 1999, 2001, 2006, 2009 and 2018.

We now zoom in to look at the differences between the years separately. When putting the high variance

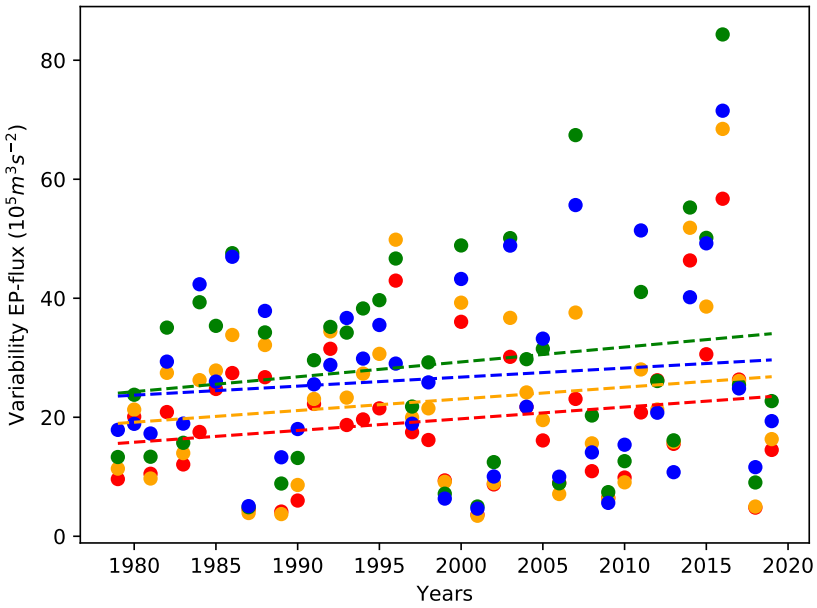

Figure 8: The variation in differences between the maximum and minimum value of the vertical component of the EP-flux [(10^5 m^3 s^{-2})] per year over the area of 90°N to 60°N. Red indicates $p = 3$ hPa, orange $p = 5$ hPa, green $p = 10$ hPa and blue $p = 20$ hPa. The trend lines have the corresponding colours.

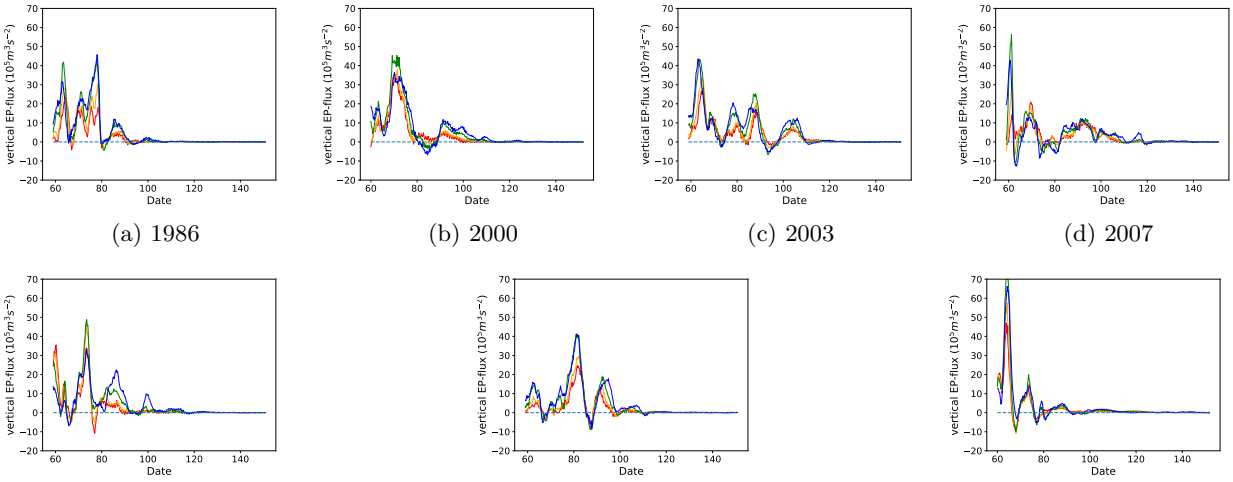

(a) 1986 (b) 2000 (c) 2003 (d) 2007

(e) 2014 (f) 2015 (g) 2016

Figure 9: Years with a high variance in the vertical component of the EP-flux over the area of 90°N to 60°N. Red indicates $p = 3$ hPa, orange $p = 5$ hPa, green $p = 10$ hPa and blue $p = 20$ hPa.

years next to each other as pictured in Figure 9, we can see that they are characterised by one or multiple very high peaks and some smaller ones, resulting in a tumultuous picture. After every relatively high peak, the wave activity drops really fast, resulting in a steep gradient. After the lower peaks, the gradient is a lot less steep. This combination of steep gradients after high peaks and the other way around, can be found for all the 41 years. When we look at the low variance years in Figure 10, this becomes even more clear. There are only a few small peaks and the gradient of all years is as good as negligible throughout all months of

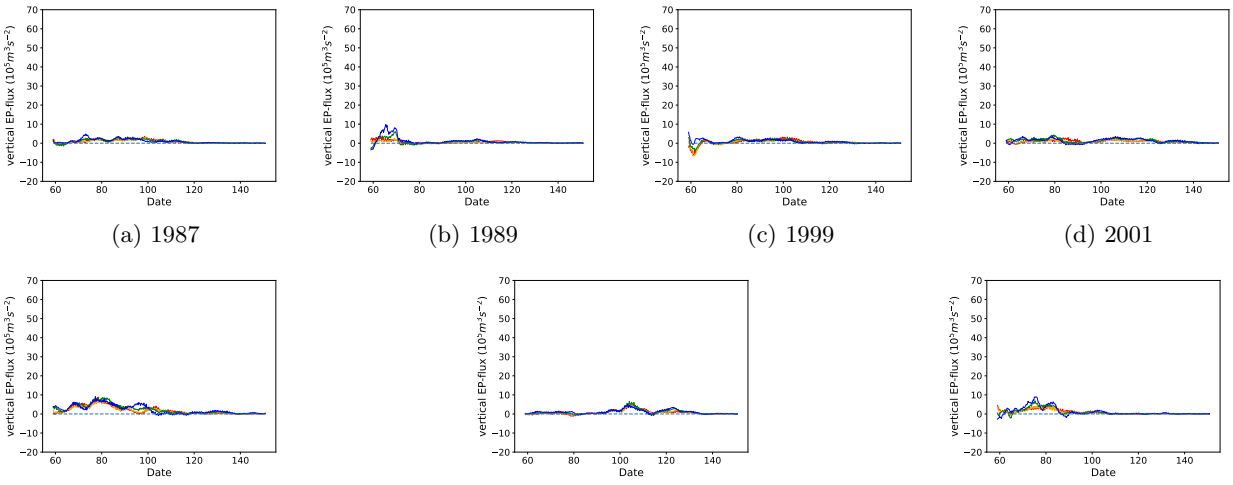

(a) 1987 (b) 1989 (c) 1999 (d) 2001

(e) 2006 (f) 2009 (g) 2018

Figure 10: Years with a low variance in the vertical component of the EP-flux. Red indicates $p = 3$ hPa, orange $p = 5$ hPa, green $p = 10$ hPa and blue $p = 20$.

March to May.

In addition to the vertical component of the EP-flux, we also look at the divergence of the EP-flux. In Figure 11a, we can see the mean divergence over the years of 1979-2019 for all five pressure levels. From this figure, we can see that in the higher stratosphere, the divergence is a lot more negative than in the lower stratosphere, indicating a stronger planetary wave drag. All levels have a positive gradient and finally end up at a divergence of zero.

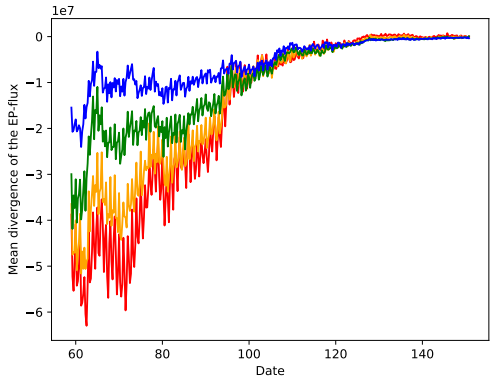

(a) Mean EP-flux divergence [ms^{-2}] over the years of 1979-2019 and over the area of 90°N to 60°N. Red indicates $p = 3$ hPa, orange $p = 5$ hPa, green $p = 10$ hPa and blue $p = 20$ hPa.

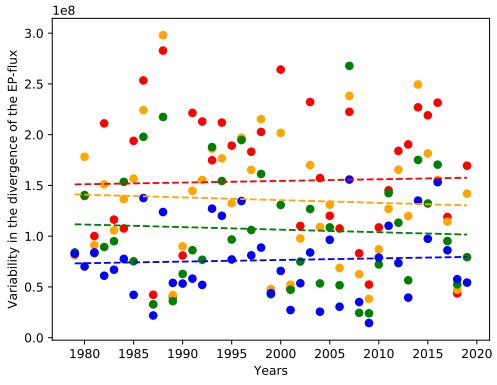

(b) The variability in the divergence of the EP-flux [ms^{-2}] over the area of 90°N to 60°N. Red indicates $p = 3$ hPa, orange $p = 5$ hPa, green $p = 10$ hPa and blue $p = 20$ hPa. The trend lines have the corresponding colours.

Looking at the trend over the years, as pictured in Figure 11b, we can see that the changes over the years in the divergence are smaller than the variability in the vertical component of the EP-flux as pictured in Figure 8. The trend lines of the five pressure levels are, from low pressure to high, 163363, -268356, -253481, 159167 and 9870 ms^{-2}year^{-1}, which are really small numbers compared to the scale of 10^8 ms^{-2} of the variability in the divergence. Their correlation coefficients are $r = 0.03 \pm 0.16$, $r = -0.05 \pm 0.16$, $r = -0.05 \pm 0.16$, $r = 0.05 \pm 0.16$ and $r = 0.01 \pm 0.16$. These very low correlations support the idea that the gradients are of

not much significance. Therefore, we thought it would be more useful to look at the divergence per month, to find possible trends in the divergence of the EP-flux.
Based on Figure 11a, we can assume that the divergence for May will be mostly zero and thus not of much interest, so we focus our attention on March and April. For both these months, we plot the mean divergence per year. The result of this can be seen in Figure 12. In a), we can see the mean divergence of March.

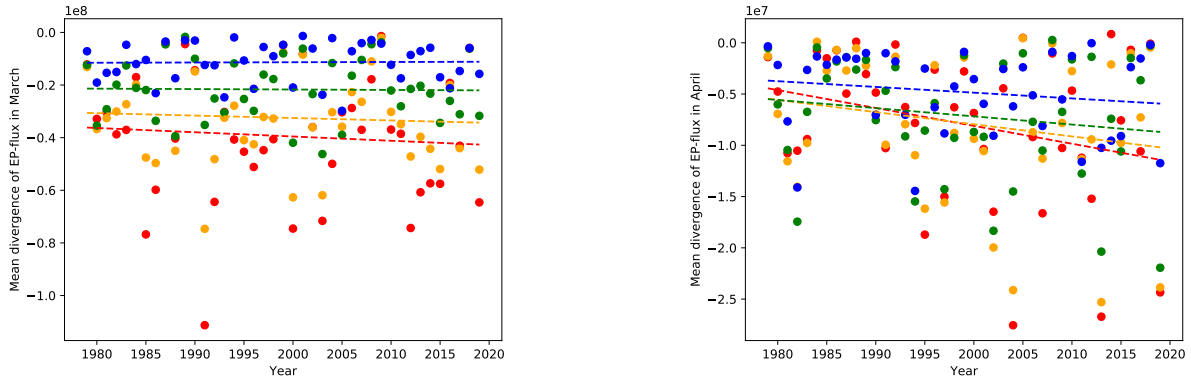

(a) March (b) April

Figure 12: The mean divergence for a) March and b) May of the EP-flux [ms^{-2}]. Red indicates $p = 3$ hPa, orange $p = 5$ hPa, green $p = 10$ hPa and blue $p = 20$ hPa. The trend lines have the corresponding colours.

The trend lines have, from low pressure to high, the following values: -161674, -92697, -16485, 9544 and -14782 ms^{-2}year^{-1}. Their correlation coefficients are $r = -0.08 \pm 0.16$, $r = -0.06 \pm 0.16$, $r = -0.02 \pm 0.16$, $r = -0.02 \pm 0.16$ and $r = -0.05 \pm 0.16$. Again, these are just very slightly negative gradients and very low correlations, except for $p = 20$ hPa, which has an even smaller positive gradient. Thus, there is no linear trend in the mean divergence for March. We can also see that the most negative divergence happens higher up in the stratosphere, just as we already could see from Figure 11a. For April, the values of the mean divergence are approximately a factor of 10 smaller than the values of the mean divergence of March. Their trend lines however, seem to have a bigger gradient. Again from low to high pressure, their gradients are -174361, -118555, -79975, -56003 and -11910 ms^{-2}year^{-1} and their correlation coefficients are $r = -0.28 \pm 0.14$, $r = -0.20 \pm 0.15$, $r = -0.16 \pm 0.15$, $r = -0.17 \pm 0.15$ and $r = -0.07 \pm 0.16$. When comparing these gradients to the gradients of March, we can see that they are bigger or comparable in size, although the values of the mean divergence are smaller. The correlation coefficients are low for April as well. So again there is not a significant linear trend for the mean divergence of April. Combining the results from March and April, we can assume that the mean values of the divergence do not change a lot, but they do extend more towards the end of April, causing lower mean divergences over the years in April. However, since the correlation coefficients are very weak, this is not a significant trend.

4.6 Northern annular mode

Next, we look at the northern annular mode index (NAM-index), averaged over multiple time scales, to see if there are any changes in the pressure distribution over the northern hemisphere. In Figure 13a, the mean NAM-index for every year is plotted. Some years are positioned more on the positive side of the index, while other fall on the negative side. The mean NAM-index over the years of 1979-2018, is 0.25 with a standard deviation of 0.40. The trend line has a gradient of 0.001 year^{-1}, which is just a very slight positive trend. The correlation coefficient is $r = 0.03 \pm 0.16$, which is very low, indicating that the trend is not linear. When we limit the months over which the NAM-index is averaged to the months of March-May, we end up with the result shown in Figure 13b. These months have a mean index value of 0.22 and a standard deviation of 0.65. There is a positive trend visible. The trend line has a gradient of 0.008 year^{-1}, which is already eight times the gradient over all months. The correlation coefficient is $r = 0.15 \pm 0.15$, which is still a weak correlation. The NAM-index over the months March to May thus seem to tend towards a higher NAM-index, but due

to the weak correlation, we cannot say there actually is a linear trend. To see the contribution of the three months to this, we plot the NAM-index averaged over the specific months, as can be seen in Figure 14 a, b and c. In Figure 14a, the average NAM-index for March is plotted. The mean value of the index is 0.43 and the standard deviation is 1.37, which are both a lot higher than the values for the mean of March to May or for the whole year. The trend line for March is 0.012 year^{-1}, which is also bigger than for March-May and for the whole year. Its correlation coefficient is $r = 0.10 \pm 0.16$, which is lower than for the months of March to May. In Figure 14b, the situation for April is plotted. Here, the mean NAM-index is 0.14 and the standard deviation is 0.77. The mean NAM-index for April is thus lower than the NAM-index for March. The trend line has a gradient of 0.011, which is about the same as for March. Its correlation coefficient is $r = 0.17 \pm 0.15$. The last month we are going to take a closer look at, is May, which can be seen in Figure 14c. The mean value of the NAM-index for May is 0.09 with a standard deviation of 0.70. This mean value is lower than the values for March and April. The trend line has a gradient of 0.002, which is also very low compared to March and April and is the same as the gradient for the mean NAM-index over the years for all months. Its correlation coefficient is $r = 0.04 \pm 0.16$, which is very weak and thus indicates no linearity.

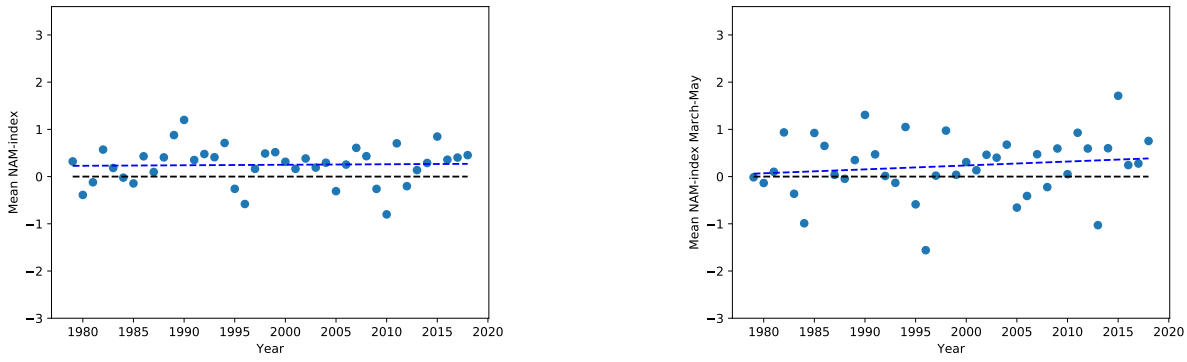

(a) (b)

Figure 13: The northern annular mode index averaged over a) a whole year and b) over the months March-May for the years of 1979-2019. The black line indicates the zero line.

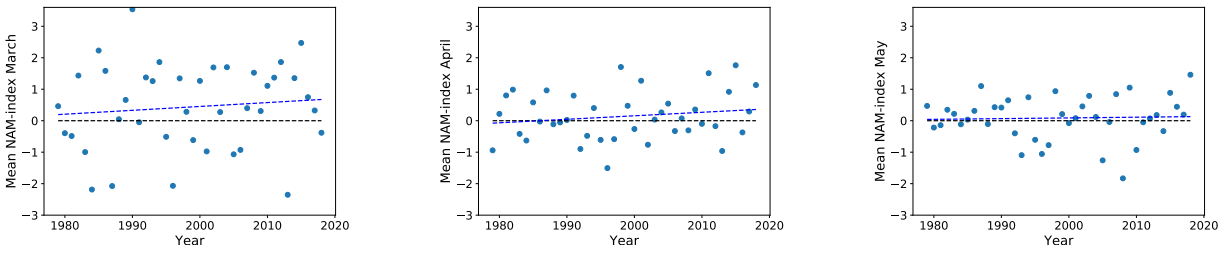

(a) (b) (c)

Figure 14: The northern annular mode index averaged over a) March, b) April and c) May for the years of 1979-2019. The black line indicates the zero line.

4.7 Correlations between the reversal date, planetary waves and the NAM

To conclude the results, we take a look at the possible correlations between the different sections discussed above. We start with the comparison of the zonal mean zonal wind reversal date to the potential vorticity anomaly reversal date at respectively $\theta = 845$ K and $\theta = 840 - 850$ K in Figure 15. It has a positive gradient of 0.88 and all the data is situated around the trend line. This results in a correlation coefficient of

$r = 0.82 \pm 0.05$, indicating a strong correlation and thus a linear relationship between the reversal date of the PV* and u. This can also be deduced from the one-to-one line plotted. We also checked this correlation for the other isentropic levels and layers. For respectively $\theta = 645$ K and $\theta = 640 - 650$ K we have a positive gradient of 0.48 and a correlation coefficient of $r = 0.47 \pm 0.12$, which is just a medium correlation instead of the strong correlation for $\theta = 845K$ and $\theta = 840 - 850$ K. For $\theta = 1045$ K and $\theta = 1040 - 1050$ K we have a gradient of 0.51 and a correlation coefficient of $r = 0.54 \pm 0.11$, which is also a medium correlation. For the last case of $\theta = 1195$ K and $\theta = 1190 - 1200$ K, we have a gradient of 0.41 and a correlation coefficient of $r = 0.40 \pm 0.13$, which is a medium correlation as well. In short, only in the middle stratospheric level of $\theta = 845$ K and layer of $\theta = 840 - 850$ K, there is a strong correlation between the zonal mean zonal wind and the potential vorticity anomaly.

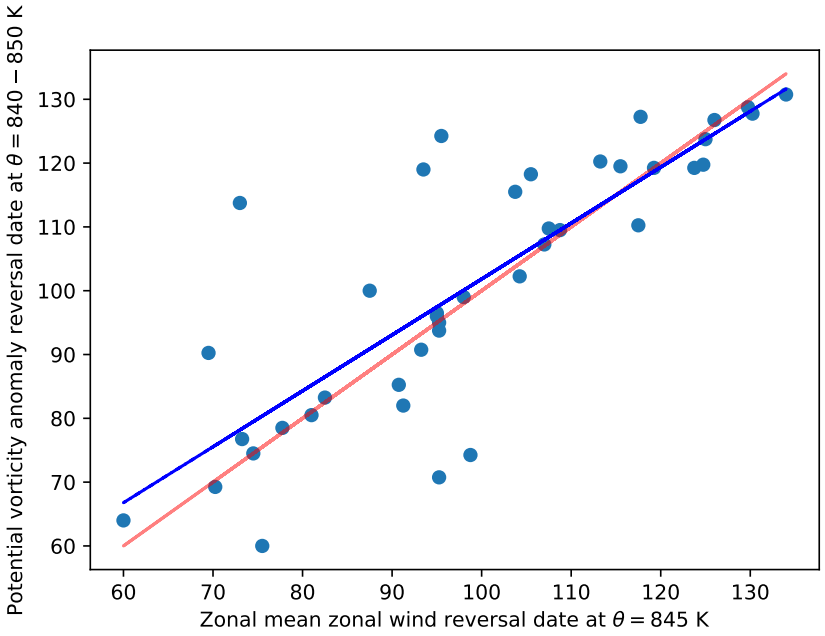

Figure 15: The reversal date of u at $\theta = 845$ K against the reversal date of PV* at $\theta = 840 - 850$ K from 1979-2019. The blue line is the trend line, the red line is the one-to-one line.

Next, we check the relationship between the PV* reversal date and the u reversal date at respectively $\theta = 840 - 850$ K and $\theta = 845$ K with the variance in the vertical component of the EP-flux as is shown in Figure 16a and 16b. Here, the u reversal has a negative gradient of -0.79 day $(10^5\ \mathrm{m^3 s^{-2}})^{-1}$ and a correlation coefficient of $r = -0.55 \pm 0.11$, which is of medium strength. The PV* reversal has an even more negative gradient of -1.08 day $(10^5\ \mathrm{m^3 s^{-2}})^{-1}$ and a correlation coefficient of $r = -0.71 \pm 0.08$, which is a strong correlation. We also looked at the correlation between the variation in the divergence of the EP-flux and the two reversal dates at the same isentropic level and layer, which are not shown due to their resemblance to the correlation between the vertical component of the EP-flux and the two reversal dates. For the relation between the divergence and u, we got a correlation coefficient of $r = -0.44 \pm 0.13$, which is of medium strength. For the divergence against the PV*, we got a correlation coefficient of $r = -0.60 \pm 0.10$, which is a strong correlation.

For the relation of the NAM-index from March to May with the variance in vertical component of the EP-flux at $p = 10$ hPa, we find the result as shown in Figure 17a. We can see that there is a slight positive trend with a gradient of 0.0045 $(10^5\ \mathrm{m^3 s^{-2}})^{-1}$, but since its correlation coefficient is $r = 0.11 \pm 0.16$, we can't say that this trend is significant or even valid. For the variance in the divergence of the EP-flux against the mean value of the NAM-index over March to May in Figure 17b, it is really visible as well that there is no linear correlation between the divergence and the NAM-index. The correlation coefficient is $r = -0.01 \pm 0.16$, which

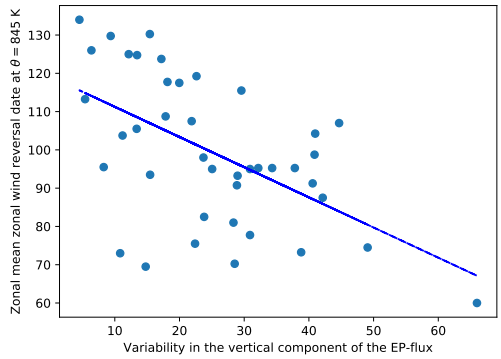

(a) The variability in the vertical component of the EP-flux [10^5 m^{3}s^{-2}] against the u reversal date at $\theta = 845$ K for 1979-2019.

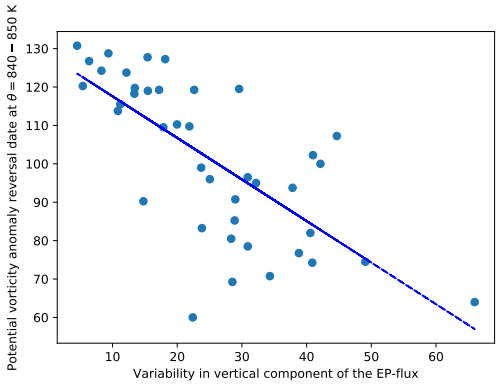

(b) The variability in the vertical component of the EP-flux [10^5 m^{3}s^{-2}] against the PV* reversal date at $\theta = 840 - 850$ K for 1979-2019.

Figure 16: See description a) and b).

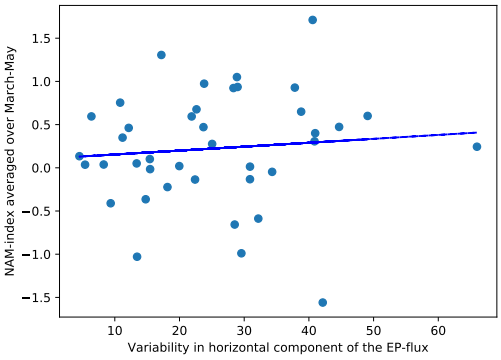

(a) The variability in the vertical component of the EP-flux [10^5 m^{3}s^{-2}] at $p = 10$ hPa against the NAM-index averaged over March-May for 1979-2018.

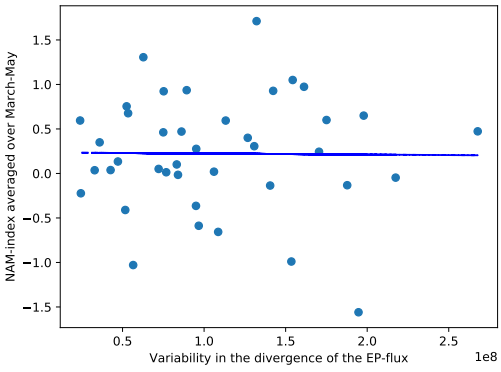

(b) The variability divergence in the EP-flux [ms^{-2}] at $p = 10$ hPa against the mean NAM-index over April for 1979-2018.

Figure 17: See description a) and b).

is very low. When looking at the correlation between other isobaric levels for the variability in the vertical component and divergence of the EP-flux and the NAM-index, no correlation could be found either.

The last ones to look at, are the relationships between the u and PV* reversal dates at $\theta = 845$ K and $\theta = 840 - 850$ K against the NAM-index. They are pictured in respectively Figure 18a and Figure 18b. Figure 18a has a correlation coefficient of $r = -0.14 \pm 0.16$ and Figure 18a has a correlation coefficient of $r = -0.08 \pm 0.16$. Both are very weak correlations and thus it can not be said that there is a linear relationship between the NAM-index and both reversal dates. When looking at the other isentropic levels and layers for the reversal dates of u and PV*, there is no linear correlation either. The strongest correlation to be found was between the reversal date of the PV* at $\theta = 1040 - 1050$ K, with $r = -0.32 \pm 0.14$, which is still a weak correlation.

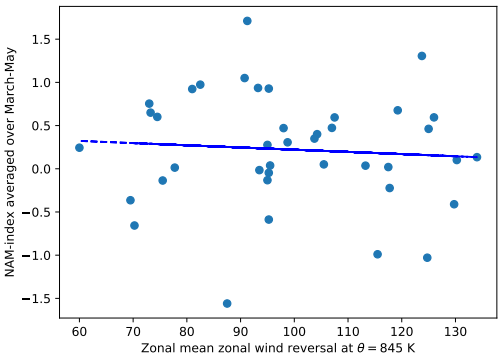

(a) The u reversal date at $\theta = 845$ K against the NAM-index averaged over March-May for 1979-2018.

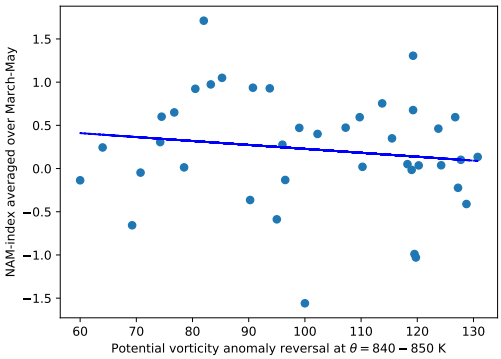

(b) The PV* reversal date at $\theta = 840 - 850$ K against the NAM-index averaged over March-May for 1979-2018.

Figure 18: See description a) and b).

5 Discussion

Based on the results described in Section 4, we can make the following observations:

5.1 The reversal day of u and PV*

Both the zonal mean zonal wind and potential vorticity anomaly have a delayed reversal date for the middle stratosphere. The higher stratosphere, at $\theta = 1190 - 1200$ K for the reversal of the PV* is the only one of which the trend line is decreasing. However, all correlation coefficients are very low and thus, in contrast to the results of Wei, Chen, and Huang [3], Sheshadri, Plumb, and Domeisen [34] and others, we can not conclude with certainty that the reversal date is delayed for either the PV* or the u. One of the reasons for this difference might be the different definitions that are used. The data set used for these researches is not the same, but this should not make such a big difference. The correlation between the PV* and u at respectively $\theta = 840 - 850$ K and $\theta = 845$ K is strong, which was to be expected due to the invertibility principle of the potential vorticity, as described in Section 2.5. For the other isentropic levels (layers), the correlation was of medium strength. When looking at the u reversal, it was found that there are two periods where more than average reversals take place. One around day 95 (6 April) and day 125 (6 May). It turns out that [17] did find this in his research as well, for the days of 28 March and 5 May. This difference is probably caused by his use of a different area, namely $65° - 75°$N, to determine the wind reversal and only demanding 5 days of westerlies after an easterly instead of the 10 days we used.

5.2 Extremely early and late reversal dates for u and PV*

The years of the extremely early and late reversal dates for u and PV* at respectively $\theta = 845$ K and $\theta = 840 - 850$ K agreed for the high majority of the years. The later years turn out to happen more after the year of 2000. The earlier years don't show such a trend, with about just as much early reversals before as after the year of 2000. This indicates a shift towards more late reversal dates over the years, while the early reversal dates show no major difference.

5.3 The propagation of the u and PV* reversal

We found that u reverses either from the stratopause to the tropopause or from the tropopause to the stratopause. Most of the time, the reversal starts in the higher stratosphere, with a mean difference of -3.25 days between the levels of $\theta = 645$ K and $\theta = 1195$ K. The PV* has a way bigger time lag between the lower and higher stratosphere of 32.57 days and thus almost always starts its reversal from the lower stratosphere. For the u reversal, all cases of extreme differences between the higher and lower stratosphere, happened from 1999 on, so there where no extreme differences in the first 20 years. For the PV* reversal, such a difference over the years could not be found. In the research paper of Wang et al. [35], a distinction was made between asynchronous and synchronous development of the reversal date of u, although on different terms. Where asynchronous corresponds to a start of the reversal in the stratopause and synchronous to a start of the reversal in the tropopause. The difference can be found in that the research of Wang et al. [35] focused was on the connection between the synchronicity and the planetary wave activity and not on potential changes over the years.

5.4 Planetary waves

The variance of the vertical component of the EP-flux seem to be slowly increasing over the years, but due to their weak correlation coefficient, it cannot be said that there actually is a linear relationship. On average, the years with higher amplitudes of EP-flux resulted in earlier onset dates for the SFW, while lower amplitudes leaded to later onset dates. This applies to both the u and the PV* reversal, showing respectively a medium and a strong correlation to the vertical component of the EP-flux. The high activity of the planetary waves mixes the potential vorticity, which in its turn affects the strength of the wind velocity according to the invertibility principle, so this result was to be expected.

The divergence of the EP-flux shows no linear trend over the years, based on the weak correlation coefficients, for neither March, April nor the average over March to May. The correlation between the variation in the divergence of the EP-flux and u was of medium strength and the correlation between the divergence and the PV* of high strength, just as for the vertical component of the EP-flux. Hu et al. [13] has looked further into the effect of planetary waves on the onset date of the SFW and concluded that the activity of the planetary waves is stronger in winters when major-SSWs happen and becomes weaker in the spring months following the major-SSW. This eventually results in later onset dates for the SFW. We did not look at the effect of SSWs in this research, but it would be interesting to see if there is a trend in the occurrence and timing of SSWs and their possible effect on the delay of the onset date of the SFW and the propagation of the u and PV* reversals.

5.5 Northern annular mode

The NAM-index over the months of March to May seemed to show a tendency towards a higher index, but looking at the correlation coefficient, which is very low, it cannot be said that there is a linear trend. We could not find a strong correlation for the mean value of the NAM-index for a full year and the separate months of March, April and May either. This is in contrast to the result of Pogoreltsev et al. [36], where it was stated that the NAM-index was showing a trend towards a more positive value. This difference might be caused by a different use or size of data sets or used definition of the NAM-index. In Section 2.4 it was stated that prior to the SFW, a prolonged period with a positive NAM-index occurs and after the SFW a period with negative values. Based on this, we expected the averaged NAM-index over the months of March to May and especially April to be more positive when the stratospheric final warming is delayed, which is not what we could extract from these results. For the relationship between the NAM-index and the two methods of measuring the planetary wave behaviour, no linear trends could be found either. For all isobaric levels against the NAM-index, the correlation coefficients where very weak.

Our last result to be evaluated is the relation between the NAM-index and the reversal dates for the PV* and u. In spite of our expectations of finding a positive correlation between both reversal dates and the NAM-index over March to May, with higher NAM-index values for later reversal dates, no linear trend between the two could be found. For all isentropic levels and layers, the correlation with the NAM-index was weak to very weak. Thus, we cannot conclude that there is a strong relationship between the stratospheric final warming and the spring amplification following the reasoning of this research. Suggestions for further research include looking at the strength of the zonal mean zonal wind and the potential vorticity anomaly in relation to the NAM-index. We also worked a lot with averages over areas and over time. Working on smaller scales to exclude those averages, might make comparisons more precise. Something that would also alter the quality of the research done, is to work with a larger data set, going further back in time.

6 Conclusion

What are the changes in the occurrence of the stratospheric final warming due to climate change and how do these changes explain the observed change in the position of stationary waves near the surface of the earth?

This was the research question we asked ourselves at the beginning of this paper. Our goal was to investigate the changes in the stratosphere in relation to the observed spring amplification in the mid-latitudes on the northern hemisphere using re-analysis. The hypothesis was that the strong warming in the spring months was connected to the delay of the stratospheric final warming. The starting point of this hypothesis is the different effect the increased amount of carbon dioxide has on the stratosphere and the troposphere. The temperature in the stratosphere decreases, while the temperature in the troposphere increases. The stratospheric polar vortex can be described by both the potential vortex anomaly and the zonal mean zonal wind velocity. It was shown by Wei, Chen, and Huang [3], Sheshadri, Plumb, and Domeisen [34] and others that the stratospheric final warming was delayed compared to the years of 1970s. In our research, we could also find a ascending trend in the trend lines for the middle atmosphere, but due to the low correlation coefficient, we can't say that this really is a linear trend over the years. What we did show, is the importance of the height chosen to measure the final warming, especially for the potential vorticity anomaly, which has a large time lag between the reversal at the lower and the higher stratosphere. For the zonal mean zonal wind reversal, it was shown that u reverses mostly around the dates of 95 (6 April) and 125 (6 May), which we call the early and late reversals. Lately, the extremely late years turn out to happen more often, while the early years stay relatively constant. The last notable change in the stratospheric final warming, is the occurrence of longer time lags between the higher and lower stratosphere for the u reversal and the other way around. Since the 2000s, these differences in the u reversal has started to become bigger. For the PV* reversal, such a trend could not be found.

Analysing the behaviour of planetary waves, we could conclude that the activity of the planetary waves played a significant role in the earlier onset dates of the SFW, while the activity did not contribute a lot to the later onset dates. For these later onset dates, it is assumed that the absorption of solar radiation plays a bigger role, and thus climate has a stronger influence in those cases. Both the vertical component and divergence of the EP-flux don't show any big differences over the years, which would explain that the early reversal dates are continuing to occur with the same frequency. The occurrence of more later reversal dates could then be an effect of the changing climate. It could also be due to a possible change in sudden stratospheric warmings happening over winter, with weaker planetary wave activity following a major-SSW and thus later final warmings, according to Hu et al. [13].

In spite of the findings of Pogoreltsev et al. [36], we could not find a linear trend in the NAM-index. Neither could there be found a linear relationship between the NAM-index over March to May and the planetary wave activity. Our final and most important result is that there is no linear relationship between the reversal dates of u and PV* and the NAM-index over March to May. We had expected that a later reversal would lead to a higher NAM-index over spring and thus to the spring amplification, but this relationship could not be validated with the use of the reversal date only.

Summarized, it could not be shown that the final warming is indeed delayed, but the later final warming are happening more often since the 2000s. There is no significant change in the activity of the planetary waves, leading us to believe that the climate plays a bigger role in a possible delay in the final warming than the activity of the planetary waves, but more research for this is needed. The mean value of the NAM-index from March to May does not show a linear trend either. The change in the position of stationary waves near the surface of the earth in the form of the NAM can not directly be explained by the onset date of the stratospheric final warming. Further research is needed to explore other influences, such as the strength of the stratospheric polar vortex and the importance of the length of the data set.

A Values for the PV* reversal on different isentropic layers

Year	$\theta = 490 - 500$ K	$\theta = 640 - 650$ K	$\theta = 840 - 850$ K	$\theta = 1040 - 1050$ K	$\theta = 1190 - 1200$ K
1979	≤59,00	≤59,00	119,00	127,25	136,25
1980	62,00	≤60,00	≤60,00	98,25	122,25
1981	≤59,00	97,00	127,75	127,25	140,50
1982	61,50	96,00	90,75	89,50	88,50
1983	60,50	59,25	90,25	120,25	139,25
1984	≤60,00	≤60,00	119,50	124,75	141,25
1985	≤59,00	68,50	80,50	83,75	131,25
1986	71,75	74,00	76,75	64,00	125,25
1987	≤59,00	≤59,00	120,25	125,25	138,75
1988	67,25	74,25	70,75	97,50	136,00
1989	≤59,00	≤59,00	115,50	118,25	126,75
1990	97,75	100,25	119,25	107,75	135,25
1991	≤59,00	88,50	99,00	85,25	86,25
1992	63,00	80,50	78,50	76,00	120,00
1993	64,00	94,25	96,50	96,75	105,25
1994	75,00	90,50	85,25	83,75	83,75
1995	75,75	81,75	95,00	95,00	95,25
1996	71,25	85,25	100,00	99,50	98,75
1997	112,25	115,75	110,25	109,25	115,75
1998	≤59,00	82,50	83,25	106,75	120,75
1999	≤59,00	≤59,00	124,25	125,50	117,75
2000	63,50	96,25	74,25	70,75	70,25
2001	≤59,00	105,25	130,75	132,25	133,25
2002	≤59,00	81,50	123,75	125,00	125,25
2003	≤59,00	99,75	102,25	103,50	103,75
2004	≤60,00	106,75	119,25	119,00	118,75
2005	68,00	70,00	69,25	116,00	126,25
2006	≤59,00	89,00	128,75	129,75	134,00
2007	≤59,00	106,00	107,25	104,00	103,25
2008	≤60,00	≤60,00	127,25	137,00	138,25
2009	≤59,00	113,50	126,75	127,75	128,25
2010	≤59,00	≤59,00	118,25	120,00	125,75
2011	92,25	95,50	93,75	93,50	93,50
2012	≤60,00	85,25	109,75	120,50	128,25
2013	≤59,00	112,25	119,75	117,00	115,50
2014	60,50	85,25	74,50	72,50	≤59,00
2015	77,75	86,50	82,00	81,50	81,50
2016	≤60,00	66,75	64,00	117,25	127,25
2017	≤59,00	61,75	96,00	95,00	129,75
2018	≤59,00	≤59,00	113,75	130,25	133,00
2019	≤59,00	104,75	109,50	109,00	108,75

Table 1: The day of the reversal of the area-weighted PV* over $60° - 90°$N for the years 1979-2019.

B Values for the u reversal on different isentropic levels

Year	495 K	645 K	845 K	1045 K	1195 K
1979	119,25	93,25	93,50	94,00	96,00
1980	117,75	96,00	75,50	60,00	96,25
1981	142,00	132,75	130,25	129,00	128,00
1982	113,00	96,75	93,25	90,00	89,25
1983	135,25	77,25	69,50	69,25	68,75
1984	147,00	115,25	115,50	117,25	118,25
1985	119,50	81,75	81,00	81,25	81,50
1986	118,25	81,50	73,25	72,50	72,00
1987	137,50	118,25	113,25	113,25	113,25
1988	108,25	96,75	95,25	95,25	95,50
1989	150,75	103,00	103,75	104,75	108,75
1990	$\geq$151,00	130,75	123,75	122,75	122,75
1991	124,75	100,75	98,00	87,50	86,25
1992	100,50	78,75	77,75	77,50	77,75
1993	103,25	101,00	95,00	94,75	95,00
1994	91,50	91,00	90,75	88,75	86,00
1995	110,25	95,50	95,25	95,00	95,00
1996	98,25	98,00	87,50	86,75	99,75
1997	123,00	118,75	117,50	115,25	114,25
1998	143,25	82,50	82,50	82,75	83,25
1999	125,25	95,25	95,50	119,75	121,25
2000	137,25	100,75	98,75	97,50	92,75
2001	$\geq$151,00	132,75	134,00	135,00	134,25
2002	130,50	126,75	125,00	124,25	124,25
2003	106,75	105,75	104,25	103,25	103,00
2004	121,50	120,00	119,25	118,50	118,25
2005	133,75	131,75	131,25	130,50	130,25
2006	136,25	130,50	129,75	129,50	129,50
2007	117,00	110,25	107,00	105,50	101,00
2008	126,00	112,75	117,75	122,50	127,75
2009	131,00	127,25	126,00	125,75	126,25
2010	127,75	117,75	105,50	79,00	79,25
2011	100,75	98,75	95,25	94,75	94,50
2012	149,25	106,75	107,50	109,25	110,50
2013	141,25	128,25	124,75	121,00	120,00
2014	142,75	107,00	74,50	73,75	60,25
2015	102,75	91,75	91,25	82,75	82,25
2016	94,50	60,00	60,00	64,50	64,25
2017	96,25	95,25	95,00	94,50	94,50
2018	129,25	101,25	73,00	74,75	121,50
2019	117,00	114,00	108,75	108,00	107,50

Table 2: The day of the reversal of the area-weighted zonal mean zonal wind over $60° - 90°$N for the years 1979-2019.

References

[1] Martin Parry et al. *Climate change 2007-impacts, adaptation and vulnerability: Working group II contribution to the fourth assessment report of the IPCC*. Vol. 4. Cambridge University Press, 2007.

[2] Shaoxiu Ma et al. "Earlier green-up and spring warming amplification over Europe". In: *Geophysical Research Letters* 43.5 (2016), pp. 2011–2018.

[3] Ke Wei, Wen Chen, and RongHui Huang. "Dynamical diagnosis of the breakup of the stratospheric polar vortex in the Northern Hemisphere". In: *Science in China Series D: Earth Sciences* 50.9 (2007), pp. 1369–1379.

[4] Michel J Rochas. "L'invention de la stratosphère". In: *La Météorologie* (2013).

[5] John Marshall and R Alan Plumb. *Atmosphere, ocean and climate dynamics: an introductory text*. Academic Press, 1989, pp. 24–25.

[6] Mark P Baldwin et al. "Weather from the stratosphere?" In: *Science* 301.5631 (2003), pp. 317–319.

[7] Roland A Madden and V Ramanathan. "Detecting climate change due to increasing carbon dioxide". In: *Science* 209.4458 (1980), pp. 763–768.

[8] D Rind et al. "Climate change and the middle atmosphere. Part I: The doubled CO2 climate". In: *Journal of the Atmospheric Sciences* 47.4 (1990), pp. 475–494.

[9] Helge F Goessling and Sebastian Bathiany. "Why CO2 cools the middle atmosphere–a consolidating model perspective". In: *Earth System Dynamics* 7.3 (2016), pp. 697–715.

[10] Darryn W Waugh and Lorenzo M Polvani. "Stratospheric polar vortices". In: (2010).

[11] Aarnout van Delden. "Atmospheric Dynamics". In: *Institute for Marine and Atmospheric Research, University of Utrecht, section* 1 (2020), pp. 170–177.

[12] Amy H Butler et al. "Defining sudden stratospheric warmings". In: *Bulletin of the American Meteorological Society* 96.11 (2015), pp. 1913–1928.

[13] JingGao Hu et al. "Seasonal timing of stratospheric final warming associated with the intensity of stratospheric sudden warming in preceding winter". In: *Science China Earth Sciences* 58.4 (2015), pp. 615–627.

[14] JR Holton. *An introduction to dynamic meteorology: Elsevier Academic Press*. Vol. 88. 2004. Chap. 12.

[15] Aarnout van Delden. "Atmospheric Dynamics". In: *Institute for Marine and Atmospheric Research, University of Utrecht, section* 1 (2020), pp. 234–241.

[16] DG Andrews and Mo E Mcintyre. "Planetary waves in horizontal and vertical shear: The generalized Eliassen-Palm relation and the mean zonal acceleration". In: *Journal of the Atmospheric Sciences* 33.11 (1976), pp. 2031–2048.

[17] JingGao Hu et al. "The boreal spring stratospheric final warming and its interannual and interdecadal variability". In: *Science China Earth Sciences* 57.4 (2014), pp. 710–718.

[18] Aarnout van Delden. "Atmospheric Dynamics". In: *Institute for Marine and Atmospheric Research, University of Utrecht, section* 1 (2020), pp. 21–23.

[19] Aarnout van Delden. "Atmospheric Dynamics". In: *Institute for Marine and Atmospheric Research, University of Utrecht, section* 1 (2020), pp. 30–37.

[20] Robert X Black and Brent A McDaniel. "The dynamics of Northern Hemisphere stratospheric final warming events". In: *Journal of the atmospheric sciences* 64.8 (2007), pp. 2932–2946.

[21] Simon H Lee and Amy H Butler. "The 2018–2019 Arctic stratospheric polar vortex". In: *Weather* (2019).

[22] Geoffrey K Vallis and Edwin P Gerber. "Local and hemispheric dynamics of the North Atlantic Oscillation, annular patterns and the zonal index". In: *Dynamics of atmospheres and oceans* 44.3-4 (2008), pp. 184–212.

[23] Brian J Hoskins, Michael E McIntyre, and Andrew W Robertson. "On the use and significance of isentropic potential vorticity maps". In: *Quarterly Journal of the Royal Meteorological Society* 111.470 (1985), pp. 877–946.

[24] Aarnout van Delden. "Atmospheric Dynamics". In: *Institute for Marine and Atmospheric Research, University of Utrecht, section* 1 (2020), pp. 201–207.

[25] Aarnout J Van Delden and Yvonne BL Hinssen. "PV-θ view of the zonal mean state of the atmosphere". In: *Tellus A: Dynamic Meteorology and Oceanography* 64.1 (2012), p. 18710.

[26] Dick P Dee et al. "The ERA-Interim reanalysis: Configuration and performance of the data assimilation system". In: *Quarterly Journal of the royal meteorological society* 137.656 (2011), pp. 553–597.

[27] Peter Howard Haynes and ME McIntyre. "On the conservation and impermeability theorems for potential vorticity". In: *Journal of the atmospheric sciences* 47.16 (1990), pp. 2021–2031.

[28] Eric R Nash et al. "An objective determination of the polar vortex using Ertel's potential vorticity". In: *Journal of Geophysical Research: Atmospheres* 101.D5 (1996), pp. 9471–9478.

[29] Amy H Butler and Edwin P Gerber. "Optimizing the definition of a sudden stratospheric warming". In: *Journal of Climate* 31.6 (2018), pp. 2337–2344.

[30] HJ Edmon Jr, BJ Hoskins, and ME McIntyre. "Eliassen-Palm cross sections for the troposphere". In: *Journal of the Atmospheric Sciences* 37.12 (1980), pp. 2600–2616.

[31] Jianping Li and Julian XL Wang. "A modified zonal index and its physical sense". In: *Geophysical Research Letters* 30.12 (2003).

[32] Jacob Benesty et al. "Pearson correlation coefficient". In: *Noise reduction in speech processing*. Springer, 2009, pp. 1–4.

[33] Derek Rowntree. *Statistics without tears*. 2000. Chap. 8.

[34] Aditi Sheshadri, R Alan Plumb, and Daniela IV Domeisen. "Can the delay in Antarctic polar vortex breakup explain recent trends in surface westerlies?" In: *Journal of the Atmospheric Sciences* 71.2 (2014), pp. 566–573.

[35] Tongmei Wang et al. "On the dynamics of the spring seasonal transition in the two hemispheric high-latitude stratosphere". In: *Tellus A: Dynamic Meteorology and Oceanography* 71.1 (2019), pp. 1–18.

[36] AI Pogoreltsev et al. "Variability of planetary waves as a signature of possible climatic changes". In: *Journal of Atmospheric and Solar-Terrestrial Physics* 71.14-15 (2009), pp. 1529–1539.